NIH Public Access
Author Manuscript
J Biomech. Author manuscript; available in PMC 2010 August 25.

Published in final edited form as:
J Biomech. 2009 August 25; 42(12): 1804–1824. doi:10.1016/j.jbiomech.2009.05.015.

ON THE BIOMECHANICS OF HEART VALVE FUNCTION

Michael S. Sacks[1], **W. David Merryman**[2], and **David E. Schmidt**[1]

[1] Engineered Tissue Mechanics and Mechanobiology Laboratory, Department of Bioengineering and The McGowan Institute, University of Pittsburgh, Pittsburgh, PA

[2] Department of Biomedical Engineering, University of Alabama at Birmingham, Birmingham, AL

Abstract

Heart valves (HVs) are fluidic control components of the heart that ensure unidirectional blood flow during the cardiac cycle. However, this description does not adequately describe the biomechanical ramifications of their function in that their mechanics are multi-modal. Moreover, they must replicate their cyclic function over an entire lifetime, with an estimated total functional demand of least 3×10^9 cycles. The focus of the present review is on the functional biomechanics of heart valves. Thus, the focus of the present review is on *functional biomechanics*, referring primarily to biosolid as well as several key biofluid mechanical aspects underlying heart valve physiological function. Specifically, we refer to the mechanical behaviors of the extra-cellular matrix structural proteins, underlying cellular function, and their integrated relation to the major aspects of valvular hemodynamic function. While we focus on the work from the author's laboratories, relevant works of other investigators have been included whenever appropriate. We conclude with a summary of important future trends.

Keywords

Heart valves; biomechanics; soft tissue mechanics; cell mechanics; mechanobiology

I – Heart Valve Physiologic Function

1.1 – Introduction

Heart valves (HVs) are fluidic control components of the heart that ensure unidirectional blood flow during the cardiac cycle. Essentially, HVs are passive tissues that are directed to open and close due to inertial forces exerted by the surrounding blood. However, this description does not adequately describe the biomechanical ramifications of their function in that their mechanics are multi-modal and their loading cycle is repeated every second. For example, they must replicate this feat with each heart beat; over a period of 70 years the reader's HVs will open and close nearly 3×10^9 times.

Anatomically, there are two types of valves: semilunar and atrio-ventricular (sometimes also known as "sigmodial"). The semilunar valves (pulmonary (PV) and aortic (AV)) prevent

For correspondence: Michael S. Sacks, Ph.D., 100 Technology drive, Room 234, University of Pittsburgh, Pittsburgh, PA 15219, Tel: 412-235-5146, Fax: 412-235-5160, Email: msacks@pitt.edu.

CONFLICT OF INTEREST

The authors have no conflict of interest, financial or otherwise, that would affect their impartiality of this work.

Publisher's Disclaimer: This is a PDF file of an unedited manuscript that has been accepted for publication. As a service to our customers we are providing this early version of the manuscript. The manuscript will undergo copyediting, typesetting, and review of the resulting proof before it is published in its final citable form. Please note that during the production process errors may be discovered which could affect the content, and all legal disclaimers that apply to the journal pertain.

NIH-PA Author Manuscript
NIH-PA Author Manuscript
NIH-PA Author Manuscript

NIH-PA Author Manuscript

NIH-PA Author Manuscript

NIH-PA Author Manuscript

retrograde flow back into the ventricles during diastole. Because of their anatomical location, they form nearly a perfect circle and have three, similarly sized leaflets (Schoen, 2005; Thubrikar, 1990) and are called semilunar due to their half-moon shape. The leaflets are attached to the vessel wall at the so-called basal attachment, with their free edges coapting to prohibit flow when closed. Neighboring leaflets meet at the highest point of their basal attachment to form a commissure. The major difference between the AV and PV, besides the dimensions of the leaflets, is that the AV has coronary artery ostioles behind two of the leaflets in the aortic wall. This feature gives rise to the nomenclature of the three AV leaflets: non coronary, right and left coronary. These openings are the source for feeding the myocardium of the heart with freshly oxygenated blood.

The atrioventricular valves, the tricuspid (TV) and mitral (MV) valves, prohibit reverse flow from the ventricle to the atrium during systole. They are more structurally complex as they are not formed of equal sized leaflets and do not have symmetrical geometries. Additionally, the leaflets of the valves are tethered to the inner walls of the ventricles by chord-like structures called chordae tendineae. These serve to prevent the valves from collapsing into the atrium during systole. There are two leaflets of the MV, the anterior, which forms a continuous connection with the non coronary leaflet of the AV, and the posterior. The TV is made up of three leaflets, all of which are of different shapes and sizes. The leaflets themselves (of all the HVs) are tapered as one moves away from the basal attachment; the porcine AV basal attachment is nearly twice as thick as the free edge (Weind et al., 2002).

The gross biomechanics of HV leaflets can be demarcated into three physical loading modes: tension, shear, and flexure. These three are imposed cyclically as the valve opens (flexure), permits blood to pass (shear), closes (flexure), and prevents the reverse flow of blood (tension). Because of the different geometries between the valve types and tethering chordae tendineae of the TV and MV, these three loading types are varied between the valves. Most of the research concerned with HV mechanics has been conducted on the AV (Adamczyk and Vesely, 2002; Billiar and Sacks, 2000b, 2000a; Christie and Barratt-Boyes, 1995; Merryman et al., 2006; Sacks et al., 1998; Vesely, 1998; Vesely and Mako, 1998; Vesely and Noseworthy, 1992) and MV (Gorman et al., 1996; Gorman et al., 2004; Kim et al., 2008; Sacks et al., 2002). The driving force behind this is likely due to the fact that these AV and MV are the most problematic valves and require surgical intervention or replacement more regularly. Additionally, many studies have been conducted with the valve in vivo under the full regime of loading required during normal (or pathological) function (Thubrikar et al., 1977; Thubrikar et al., 1979; Thubrikar et al., 1977; Thubrikar et al., 1980; Thubrikar et al., 1980; Thubrikar et al., 1979, 1981; Thubrikar et al., 1986). Therefore, a complete understanding of the three individual loading modes on each valve at the present time is quite unclear.

Shear stress and flexure are difficult to measure with the valve in situ, and accurate values for what the valves *actually* experience are not currently known; however, estimates for shear stress on the AV of 10–80 dynes/cm^2 (Weston et al., 1999) and flexure in native and bioprosthetic valves (Mirnajafi et al., 2005; Mirnajafi et al., 2006) have been made recently. It is reasonable to suspect that the shear stress and flexure experienced by each valve are comparable. The normal physiological transvalvular pressures (TVP) on the valves of a heart at rest are as follows: TV, 25 mmHg; PV, 10 mmHg; MV, 120 mmHg; and AV, 80 mmHg (Guyton, 1976). These values reveal that the left side heart valves experience 5 to 8 fold higher TVPs, which are not equilibrated by the tissue thickness (left side HVs are about 2x thicker) via a simple Law of Laplace calculation.

1.2 - Heart valve disease

According to the American Heart Association (Thom et al., 2006), valvular heart disease resulted in 19,989 deaths directly and was a contributing or underlying cause of death in 42,590

NIH-PA Author Manuscript

NIH-PA Author Manuscript

NIH-PA Author Manuscript

cases in 2003. Of the mortality or contributing mortality numbers, AV disease was the most prevalent with 12,471 and 26,336 cases, respectively; MV disease cases were responsible for 2,759 deaths and 6,600 contributory deaths. Right side valve cases were significantly less (PV: 11 deaths and 35 contributory deaths; TV: 16 deaths and 69 contributory deaths). It is estimated that in 2003 there were 95,000 inpatient valve procedures performed. These numbers indicate that valvular disease is very prevalent and life threatening and additionally that the AV is the most diseased with the highest rate of morbidity.

There exist two types of valvular heart disease: congenital and acquired (Otto, 2004). Congenital valve disease is an abnormality that develops before birth and this subset of patients are who would most likely benefit most from a tissue engineered heart valve. The result of the defect may be related to improper valve size, malformed leaflets, or an irregularity in the way the leaflets are attached. This most often affects the AV or PV. A very common congenital defect is bicuspid AV disease where instead of the normal three leaflets or cusps, the bicuspid AV has only two. Acquired valve disease pertains to problems that develop within valves that were at one time normal. This is typically referred to as age-related degenerative valve disease. In the early part of the 20^{th} century, the primary cause of acquired valve disease stemmed from rheumatic valve disease; however, this trend has changed dramatically with a decrease in rheumatic valve disease and a concomitant increase in age-related degenerative valve disease (Otto, 2004).

1.3 – Focus of this review

As in many physiological systems, one can approach heart valve biomechanics from a length scale approach, since mechanical stimuli occur and have physiological impact at the system, organ, tissue, and cellular scales (Fig. 1). Yet, despite its clinical importance, the unique and demanding valvular biological/biomechanical environment is relatively unexplored, with most research focusing on valvular prosthetic design. Thus, the focus of the present review is on *functional biomechanics*, referring primarily to biosolid as well as several key biofluid mechanical aspects underlying heart valve physiological function. Specifically, we refer to the mechanical behaviors of the extra-cellular matrix structural proteins, underlying cellular function, and their integrated relation to the major aspects of valvular hemodynamic function. While not an exhaustive review, the works of most investigators known to the authors have been included. We conclude with a further aim to underscore important future trends. Finally, while the literature is extensive, there are still many gaps. Therefore, in this review we note that experimental data and theoretical models may only exist for certain valves (or even specific leaflets).

2 – Heart valve hemodynamics and fluid-structure interactions

2.1 - Heart valve hemodynamics

The mechanisms ensuring the proper function of the heart valves are essentially controlled by the surrounding hemodynamic environment. Understanding the interactions between the heart valves and the local hemodynamic environment is thus critical to better understand normal valve function and disease progression. Although the four heart valves present profoundly different anatomies and functional (e.g. opening/closing) characteristics, they all essentially function to facilitate the unidirectional flow of blood while maximizing flow rate and minimizing flow resistance. Thus, in the following we focus on AV hemodynamics as an example for all the heart valves. We also note that the effects of valve size or effective orifice area will affect the specific flow behaviors. However, for the purposes of the present review we focus on general behaviors common to valve function.

NIH-PA Author Manuscript

NIH-PA Author Manuscript

NIH-PA Author Manuscript

The AV opens during systole when the ventricle is contracting and then closes during diastole as the ventricle relaxes. In healthy individuals, blood flows through the aortic valve accelerating to a peak value of 1.35 ± 0.35 m/s (Otto, 2001). The valve closes near the end of the deceleration phase of systole with very little reverse flow through the valve. The adverse axial pressure differences causes the low inertial flow in the developing boundary layer along the aortic wall to decelerate then to reverse direction, resulting in vortices in the sinuses behind the aortic valve leaflets (Reul and Talukder, 1989). This action is thought to facilitate movement of the AV cusps (leaflets) away from the sinus wall and toward the closed position. When this force is coupled with the vortices that push the leaflet surfaces toward the closed position, a very efficient and fast closure is obtained. *In vitro* studies have shown that the axial pressure difference alone is sufficient to close the valve (Reul and Talukder, 1989).

Thus, without the vortices in the sinuses the valve still closes, but its closure is not as efficient as when the vortices are present. However, we note that the AV should functionally be considered part of the entire left ventricular outflow track. Thus, while the presence of the aortic sinuses helps to induce local hemodynamic patterns that facilitate AV function, they may have other functions. For example, during the cardiac cycle the AV annulus expands and contracts, which clearly alters how the AV leaflets function, possible facilitating valve opening. Further, the tissue structures at the leaflet/sinus interface reveal a gradual transition from the collagen rich leaflet tissue to the elastin rich sinus wall (Thubrikar, 1990). Thus, the sinus geometry may also help reduce the effects of flexural stresses at the leaflet/sinus interface. We should always thus keep in mind that various valvular components have multiple functions and interact in a complex but ultimately functionally efficient manner (see next section).

2.2 - Dynamic leaflet deformations

Clearly, a major part of understanding valve dynamics requires knowledge of the dynamic deformations that occur during valve function. Along these lines, investigators have undertaken the task of studying MV dynamics and left ventricular fluid mechanics (Bellhouse and Bellhouse, 1969; Hartiala et al., 1993; Ming and Zhen, 1986; Ormiston et al., 1981; Otsuji et al., 1997; Reul and Talukder, 1989; Schwammenthal et al., 1994). However, due to the complexity of valve anatomy, it is difficult to theoretically determine the functional role and importance of each individual component (Arts et al., 1983). Computational models, such as those described in the next section represent an exciting approach, but have not yet progressed to the point where fully dynamic function can be simulated. Moreover, simulations are currently difficult to fully validate *in vivo* with available imaging technologies. Several approaches have been taken to attempt to quantify valvular dynamics, including in-vivo (see (Sacks and Yoganathan, 2007) for details) and in-vitro approaches using in-vitro simulated flow conditions (He et al., 2005; He et al., 2003; Sacks et al., 2006; Sacks et al., 2002).

The highly dynamic motions, large anisotropic deformations, complex surface geometries, and thin leaflets clearly puts heart valve imaging beyond the forefront of what is possible with current imaging technologies. Recently, use of sonomicrometry technology has allowed greater insight into the actual in-vivo deformation patterns of the major valve structures (Eckert et al., submitted; Sacks et al., 2006). Specifically, the anterior leaflet of nine Dorsett sheep (35–45 kg) was instrumented with nine 1 mm hemispherical piezoelectric transducers in a 15 mm square array (Fig. 2-a). 3D crystal spatial positions were recorded at 250 Hz over several cardiac cycles, with peak LV pressures varied from 90 mmHg to 200 mmHg. The in-surface Eulerian strain tensor was computed from the crystal displacements. Since the central region demonstrated generally homogeneous strains, and thus we elected to focus the present study on the results from this region. To quantify the net change in leaflet dimensions the areal strain was defined as the change in the area defined by the sonocrystals expressed as percent reference area.

NIH-PA Author Manuscript

NIH-PA Author Manuscript

NIH-PA Author Manuscript

Perhaps the best way understand the key characteristics of valve deformations is to examine the simple relation between trans-valvular pressure and areal strain (Fig. 2-a). Here, one can easily observe very large changes in area (30%) under minimal trans-valvular pressure. Then, a sharp transition is observed accompanied by a highly stiff region corresponding to the coapted, fully pressurized state. Corresponding changes in areal strain with time demonstrated overall smooth deformations, with complete loading of the leaflet occurring in ~50 ms and peak strain rates of 1000%/sec (Fig. 2-b). We should note that valve tissue straining actually occurs over the entire cardiac cycle. Moreover, in a real sense a common reference state for the entire valve leaflet may not truly exist, given the high degree of spatial heterogeneity and constant changing dynamic fluid stresses. However, as a working definition for strain calculations we refer to point of initial contact between the leaflets, but before any significant coaptation can occur. For the aortic valve, we have defined this to be when a transvalvular pressure of ~4 mmHg exists (Sacks et al., 1998), whereas for the central point of the mitral valve anterior leaflet we have utilized the point of minimal LV pressure (Sacks et al., 2006).

In addition to leaflet deformation, the surrounding annulus can have a profound influence on valvular dynamics. We have recently investigated the in vivo annular kinematic data collected from surgically implanted sonocrystals in an ovine model and utilized quintic order hermite shape functions with C^2 continuity (Eckert et al., submitted) to determine the resulting strain and strain rate information along the entire annulus length (Fig. 2-c). Annular strain was shown to be regionally and temporally variant with minimum and maximum stretch values of near −15% and 6%, respectively, observed. Such information confirms the highly dynamic nature of the MV annulus and may be related to the varied fibrous-muscle structure of the annulus. Moreover, it can lay the basis for dynamic computational models of mitral valve function by allowing for prescription of the annular deformations as a time-varying boundary conditions.

Similarly, studies of normal and pathological aortic root dynamics are limited due to difficulties in performing in-vivo studies (Thubrikar et al., 1993). Dagum et al. (Dagum et al., 1999) have studied the deformation modes of the left, right, and noncoronary aortic root regions using radiopaque markers implanted at the top of the 3 commissures (sinotubular ridge) and at the annular base of the 3 sinuses. Not surprisingly, they determined that the ovine aortic root undergoes complex, asymmetric deformations during the various phases of the cardiac cycle, including elongation, compression, shear, and torsional deformation. Moreover, these deformations varied significantly among the left, right, and noncoronary regions.

Taken as a whole, these responses underscore common behaviors in all valvular tissues, and demonstrate the basic functional requirements at the tissue level:

1. Leaflets (or cusps) cycle between the fully unloaded to fully loaded state every cardiac cycle, unlike other connective tissues that remain preloaded (e.g. blood vessels).
2. Leaflets (or cusps) experienced large, anisotropic stretches during closure in response to respond to small trans-valvular pressure gradients.
3. Corresponding tension levels have been estimated to be in the range of 50 to 100 N/m during peak loading.
4. Peak strain rates are very high, reaching values of 1000%/sec.
5. Once the valve is closed, further leaflet deformation ceases.
6. Valve tissue deformations are highly sensitive to the deformations of the surrounding tissues.

Clearly, the demands on the constituent tissues are substantial to meet these physiological demands. The underlying tissue and cellular basis for these responses are discussed in Sections 3 and 4.

NIH-PA Author Manuscript

NIH-PA Author Manuscript

NIH-PA Author Manuscript

2.3 - Heart valve fluid-solid interactions

Finite element analysis has been the popular technique employed to determine the stress distribution on the leaflets of native and bioprosthetic valves with the blood pressure applied as the load on the leaflets (Kunzelman et al., 1993; Kunzelman et al., 1994; Kunzelman et al., 1998). Such analyses have also been employed to perform stress analysis with native aortic and mitral valves (Grande et al., 1998; Kunzelman et al., 1998). Numerical simulation of native heart valve function is quite challenging, with the necessity of addressing several difficult issues. It is necessary to incorporate the non-linear anisotropic mechanical properties of the leaflets and compute the complex motion of the leaflets due to the external load imparted by the surrounding fluid. In modeling the valve function, the fluid domain is most conveniently described using the Eulerian reference frame in which the fluid moves through a fixed mesh. A Lagrangian formulation is more appropriate for the leaflet motion in which the mesh moves together with the leaflet. The complete simulation of the heart valve function requires a fluid-structure interaction simulation and the two formulations are incompatible for such an analysis.

Two methods have generally been employed to circumvent this problem. De Hart (De Hart et al., 2003) utilized the Lagrange multiplier based fictitious domain method to describe the large leaflet motion within the computational fluid domain. This method is applied to a three-dimensional finite element model of a stented aortic valve. Results show that during systole the leaflets appear to be moving with the fluid in an essentially kinematical process governed by the fluid motion. The second approach is the arbitrary Lagrangian-Eulerian (ALE) method in which the computational mesh is allowed to deform (Lai et al., 2002) and move in space arbitrarily to conform to the moving boundaries and has also been successfully employed in the heart valve simulation. Recently, Vigmostad et al. (Vigmostad et al., 2008; Vigmostad et al., 2008) developed a partitioned, sharp interface approach (Marella et al., 2005) to overcome some of these limitations and employed physiologic Reynolds numbers, realistic material properties, and highly resolved grids. A partitioned approach was chosen, in which blood flow was computed using computational fluid dynamics, structural deformation was computed using an FE solver, and an FSI algorithm was developed to strongly couple these solutions. The standard governing equations for a viscous, incompressible fluid were employed to compute flow. These equations were discretized using a sharp interface, Cartesian grid, finite difference method (Marella et al., 2005). Boundaries and the embedded valve leaflets were represented using level sets, which move freely through the mesh without complex re-meshing. To decrease computation time, both local mesh refinement (LMR) and parallel algorithms were implemented. Using LMR, the Cartesian mesh was automatically refined or coarsened locally based on flow and boundary criteria to efficiently enable accurate results. With parallel processing, the solution was apportioned into multiple processors to enable high resolution without high computation times. Deformation and stresses in the valve leaflet were computed using a finite element model (FEM).

In 3D, an enhanced strain element was used to define the leaflet and membrane, bending, and shear stresses were computed as the leaflet deformed. The leaflet material model utilized a Fung-elastic model that incorporated the effects of in-plane shear and local material axes as defined by the local fiber preferred directions was employed to describe the valve leaflet in 3D, based on work by Sun et al. (Sun et al., 2005; Sun and Sacks, 2005). The FE model used a Lagrangian mesh which describes the leaflet geometry using an 8-node continuum element, and the stress and deformation of the leaflet were computed based on the leaflet properties and governing principles of solid mechanics. Inertial effects of the leaflet were incorporated, and through the no-slip condition were reflected in the flow solution. In order to couple the effects of the blood flow with those of the deforming valve leaflet, a fluid structure interaction method was developed. At every time step, a level set field was developed on the Cartesian grid to describe the current location of the valve leaflet. Based on the current conditions, the flow field

NIH-PA Author Manuscript

NIH-PA Author Manuscript

NIH-PA Author Manuscript

was computed, incorporating the leaflet velocity at the previous time step as a boundary condition, so that no-slip was enforced. The pressure and stress in the fluid were computed at the leaflet interface and were used as boundary conditions on the leaflet FE mesh. The leaflet deformed accordingly, and this deformation was fed back to the fluid and the computation continues.

Results for the leaflet shape during valve opening for a 2D FSI simulation and 3D FEM computations (Kim et al., 2008) show good agreement with 3D experimental results (Iyengar et al., 2001), (Fig. 2). The leaflet profile at the fully open position shows good qualitative agreement between the various studies. These computations were performed using high resolution grids, to enable a more accurate solution. This was achieved with the use of LMR and a parallel algorithm, and stability and efficient convergence was ensured through the use of the partitioned, sub-iteration FSI approach, and underscores the importance of the use of physiologic material properties in modeling valve dynamics.

Two simulations were performed which employed the same boundary conditions, but the material properties of the leaflet were different. Valve 1 used the material properties used by de Hart et al. (De Hart et al., 2000), while Valve 2 used actual pericardial heterograft mechanical properties (Sun and Sacks, 2005). It was noted that the pressure contours (Fig. 3) a build-up of pressure for Valve 1, which was not observed in Valve 2. This was due to the high resistance to deformation offered by Valve 1, whereas Valve 2 utilizing a more realistic material model did not offer the same resistance to flow. Figure 3(C–D) shows the axial velocity in the two valves at the same time point. Note the large jet formed by Valve 1, due to the high stiffness of the valve. Valve 2 did not have such a jet, as it offered far less resistance to flow. Although the average displacement of the two leaflets was similar, a very different opening profile was visible. Additionally, the flow fields in the two cases were vastly different. This demonstrated how important physiologically realistic leaflet material properties were for the flow field computations and ultimately for understanding valve failure.

3 – Tissue level structure and mechanical behavior

3.1 – Tissue structure and composition

Given the physiological demands on the constituent tissue structures of the heart valve and the available biological materials (e.g. collagens, elastin, proteoglycans, etc), it would seem intuitive that a single, thin collagenous membrane would suffice to form the valve leaflets. Yet, nature has evolved a tri-layered leaflet structure (Schoen, 1997; Thubrikar, 1990). The two main connective tissue layers are the fibrosa and ventricularis (Figs. 4-a,b). The fibrosa is the thickest layer and consists primarily of a dense network of type I collagen fibers. Functionally, it appears to be the main load bearing layer and extends over the entire leaflet surface. As its name implies, the ventricularis (or atrialis for the MV and TV) layer faces the left ventricular chamber (or the left and right atria in the mitral and tricuspid valves, respectively). It is composed of a dense network of collagen and elastin fibers (Vesely, 1998) (Figs. 4-c,d). The elastin fibers within the ventricularis (or atrialis) appear to be radially aligned, as evidenced by their long, fibrous appearance in radial cross-sections (Fig. 4-d). Thus, its physiological function appears to assist in reducing large radial strains that occur during maximum forward flow when the valve is fully opened.

In contrast, the central spongiosa layer contains a high concentration of highly hydrated GAGs and PGs, which are believed to lubricate the fibrosa and ventricularis as they shear and deform relative to each other during leaflet bending and pressurization (Simionescu et al., 2003). Although they are most apparent in the spongiosa, GAGs and PGs are also found throughout the leaflet. It has been demonstrated by transmission electron microscopy that the majority of GAG are located in the interfibrillary spaces (Rothenburger et al., 2002; Simionescu et al.,

NIH-PA Author Manuscript

NIH-PA Author Manuscript

NIH-PA Author Manuscript

2003), where they are likely present as components of large proteoglycans such as versican and versican-hyaluronan aggregates (Grande-Allen et al., 2004). GAGs are also visible in specific association with collagen fibrils (Rothenburger et al., 2002; Simionescu et al., 2003), in which they extend orthogonally from the fibrillar surfaces and bridge adjacent fibrils (Liao and Vesely, 2004; Liao et al., 2007). In addition to their mechanical functions, valvular GAGs and PGs are also speculated to have biological activity in regulating the sequestration of soluble mediators such as growth factors (Latif et al., 2005). The hydrated nature of most GAGs would enable the diffusion of nutrients and oxygen through the valvular tissue, which is largely avascular in adults (Duran and Gunning, 1968), to the resident interstitial cells (See section 5).

It is well known that collagen fibers can withstand high tensile forces, but have low torsional and flexural stiffness. Thus, directions in which the fibers are oriented can be identified with the directions in which the tissue is able to withstand the greatest tensile stresses. To quantify the gross fiber architecture of the valve leaflet, we used small angle light scattering (SALS) (Sacks et al., 1997). To simulate on the changes to aortic valve leaflet structure with increasing trans-valvular pressure, fresh porcine aortic valves were fixed at trans-valvular pressures ranging from 0 mmHg to 90 mmHg. Overall, increasing trans-valvular pressure induced the greatest changes in fiber alignment between 0 and 1 mmHg, and past 4 mmHg there was no detectable improvement in fiber alignment. Recently, we have quantified the amount of collagen fiber crimp in the native pulmonary and aortic heart valves (Joyce et al., 2009). Following Hilbert et al. (Hilbert, 1990; Hilbert et al., 1986), we represented the amount of collagen crimp as a percentage of the histological cross-sectional area containing observable crimp structures for each transvalvular pressure level. In this approach, cross-sectional regions displaying observable crimp were identified and the resultant areas measured, and expressed as a percentage of the total cross-sectional tissue image. It was found that at 0 mmHg ~60% of the AV transverse cross-sectional area was occupied by crimp structure. As transvalvular pressure increased, the percent crimp decreased rapidly until 20 mmHg, with minimal decreases in percent crimp thereafter. Thus, we can see that for the valvular structures much of the observed change in collagen structure is due to straightening of the collagen fibers. This is a finely tuned affair; straightening must occur at the right strain level and at the right rate to facilitate coaptation, yet not allow excessive tissue deformations that may lead to regurgitation (e.g. Fig. 2-a).

3.2 - Key biomechanical behaviors of valvular tissues

The results of the preceding section suggest a complex structure-mechanical behavior and interactions for heart valve leaflets. While there have been a few studies on MV tissue (May-Newman and Yin, 1995, 1998), most of the research concerned with HV mechanics has been conducted on the AV (Adamczyk and Vesely, 2002; Billiar and Sacks, 2000b, 2000a; Christie and Barratt-Boyes, 1995; Merryman et al., 2006; Sacks et al., 1998; Vesely, 1998; Vesely and Mako, 1998; Vesely and Noseworthy, 1992) and MV (Gorman et al., 1996; Gorman et al., 2004; Sacks et al., 2002; Stella et al., 2007). The driving force behind this is likely due to the fact that these AV and MV are the most problematic valves and require surgical intervention or replacement more regularly. Although common to all valves, the different valve geometries and effects of tethering by chordae tendineae in the TV and MV, the magnitudes and rates of these loading modes will vary between the valves. It is thus useful to divide the study to the tissue-level biomechanics of HV leaflets into in-plane stretch and flexural deformation modes. These occur cyclically as the valve opens (flexure), experiences surface shear stress from the local blood flow, followed by closure (flexure) then coaptation and full loading (tension). Therefore, behaviors of the individual loading modes are presented in the following. While we and others have made extensive examinations of other heart valve leaflets (also referred to as a “cusp,” but we consider “leaflet” a better term to describe its function), we focus here on the native aortic valve as an example of the intricacies of heart valve leaflet tissue biomechanics.

NIH-PA Author Manuscript

NIH-PA Author Manuscript

NIH-PA Author Manuscript

In-plane responses—The mechanics of soft tissues are well known to be complex: they exhibit a highly non-linear stress-strain relationship, undergo large deformations, complex viscoelasticity, and complex axial coupling behaviors that defy simple experiments and material models (Fung, 1993; Sacks, 2000). Much of this behavior is a direct result of changes in their internal structure with strain, which involves both straightening of highly crimped collagen fibers and rotation of these fibers toward the stretch axis. For valvular tissues, most previous work on the mechanical properties of the native and chemically treated aortic valve has relied on uniaxial mechanical testing (Lee et al., 1984), (Lee et al., 1984), (Vesely and Noseworthy, 1992). These studies demonstrate that chemical fixation of intact valves, especially under pressure, alters the mechanical properties of the leaflets. Marked decreases in the extensibility are generally attributed to "locking" the collagen fibers in the uncrimped state (Broom and Christie, 1982), (Christie, 1992). Tests on thin tissue strips however, cannot mimic the heterogeneous multi-axial deformation fields, combined loading sequences, and native fiber kinematics found in the physiological environment. Mayne et al. (1989) and Christie et al. (1995) have performed equi-biaxial testing (i.e. equal levels of tension applied to each test axis) that overcomes many of the above limitations of uniaxial loading. However, derivation of a constitutive relationship solely from equi-biaxial test data is limited due to multiple co-linearities that confound the ability to obtain reliable, unique model parameter values (Brossollet and Vito, 1995).

Billiar and Sacks (2000a) generated the first complete biaxial mechanical data necessary for constitutive modeling aortic valve leaflet (See Section 4). Due to the small size and heterogeneous structure of the aortic valve leaflet, testing methods were developed and validated. Leaflet specimens were subjected to biaxial tests utilizing multiple loading protocols to provide a range of loading states that encompass the physiological loading state. The leaflets demonstrated a complex, highly anisotropic mechanical behavior (Fig. 5-a), including pronounced mechanical coupling between the circumferential and radial directions. The MV anterior leaflet, produced similar albeit less anisotropic response (Fig. 5-b). Mechanical coupling between the axes produced negative strains along the circumferential direction and/or non-monotonic stress-strain behavior when subjected to equi-biaxial tension, a behavior noted by Mayne et al. (1989) but was not explained. Moreover, Adamczyk et al. (Adamczyk and Vesely, 2002) measured AV leaflet strains in-situ and found that negative strains can occur in the non-coronary leaflet.

Time dependent behaviors—The above studies focused on the elastic behavior of valvular tissues. There are substantial previous studies using uniaxial testing techniques which have investigated stress-relaxation in valvular tissues and modeled the response using quasi-linear viscoelastic theory (Carew et al., 2000; Carew et al., 1999). However, time dependent behaviors under physiological multi-axial loading states have only recently been quantified. We have conducted novel sub- to physiological strain rate studies under biaxial stretch on the AV and MVAL (Grashow et al., 2006a; Grashow et al., 2006b; Stella et al., 2007). The resulting stress–strain responses were found to be independent of strain rate for both valve leaflets, as was the observed low level of hysteresis (Fig. 5). Stress relaxation and creep results indicated that while the leaflet tissues exhibited significant stress relaxation, they exhibited negligible creep over the three hour test duration. To our knowledge, this response is unique in the biomechanical literature and stands in contrast, for example, to that reported for other dense collagenous tissues such as tendon and ligament (Provenzano et al., 2001; Thornton et al., 2001; Thornton et al., 1997).

However, the underlying micro-structural basis for this unique mechanical behavior is presently unknown. As collagen is the major structural component of the MVAL, we investigated the relation between collagen fibril kinematics (rotation and stretch) and tissue-level mechanical properties in the MVAL under biaxial loading using small angle x-ray

NIH-PA Author Manuscript

NIH-PA Author Manuscript

NIH-PA Author Manuscript

scattering (SAXS). A novel device was developed and utilized to perform simultaneous measurements of tissue level forces and strain under a planar biaxial loading state. Collagen fibril D-period strain (ε_D) and the fibrillar angular distribution were measured under equibiaxial tension, creep, and stress relaxation to a peak tension of 90 N/m. Results indicated that, under equibiaxial tension, collagen fibril straining did not initiate until the end of the nonlinear region of the tissue-level stress-strain curve. At higher tissue tension levels, ε_D increased linearly with increasing tension. Changes in the angular distribution of the collagen fibrils mainly occurred in the tissue toe region. Using ε_D, the tangent modulus of collagen fibrils was estimated to be 95.5 ± 25.5 MPa, which was ~27 times higher than the tissue tensile tangent modulus of 3.58 ± 1.83 MPa. In creep tests performed at 90 N/m equibiaxial tension for 60 minutes, both tissue strain and ε_D remained constant with no observable changes over the test length (Fig. 6-a). In contrast, for stress relaxation performed for 90 minutes, ε_D was found to rapidly decrease in the first 10 minutes followed by a slower decay rate for the remainder of the test (Fig. 6-b).

It is interesting to note that we also evaluated the measured the strain during the relaxation tests. First, our device was able to resolve stretch values to 0.001 or 0.1% (Grashow, 2005). We found that during relaxation experiments the circumferential strain increased by 0.1% (i.e. within measurement error) and the radial component to 0.4%. If the relaxation was an artifact of excessive deformation resulting from the stress concentrations near the sutures, then the strain in the central region should decrease, which it did not. Thus, we have no evidence of decreasing strain due to stress concentrations or other experimental artifacts.

Overall, our results suggest that:

1. Since stress relaxation occurred at both the tissue and fibril levels, it may be a result of an internal slipping mechanism, possibly modulated by non-collagenous components (e.g. proteoglycans).
2. The lack of creep but the occurrence of stress relaxation suggests the internal slipping can only occur when the external strains are held constant, not under constant loads.
3. Overall, while valvular tissues exhibit intrinsic viscoelastic behavior these behaviors do not appear to be functional.

Taken as whole, these results support our observations that valvular tissues are *functionally anisotropic, quasi-elastic biological materials*. These mechanical qualities also appear to be unique to valvular tissues; indicating an ability to withstand loading without time-dependent effects under physiologic loading conditions.

Flexural response—Any biomechanical study of heart valve leaflets must be designed to elucidate the unique mechanical properties of the tri-layered aortic cuspal structure. This is especially important when determination of the layer mechanical properties of the compliant cuspal tissue in the low stress-strain region is considered. For example, while biaxial mechanical testing techniques successfully quantified the in-plane stress-strain response (Sacks, 2000), they cannot determine the contributions of individual layers. Further, although the cuspal displacements are large the tissue strains are actually small, so that the low strain region of stress-strain curve is of interest. Mechanical properties in the low strain region are difficult to obtain accurately from tensile studies, which also cannot measure compressive stiffness. Flexure represents not only a natural deformation mode of the valve leaflet, it also introduces a deformation mode in which the different layers (unlike uni- or biaxial tensile experiments), experience different strains. Further, the stress-strain response of the individual cuspal layers in the low strain region under both tension and compression can be obtained without the need for dissection or other interventional approaches. Flexure of soft biological materials offers two distinct advantages over tensile mechanical testing: 1) the ability to discern slight changes in stiffness at low-stress strain levels that would not be appreciable in tension

NIH-PA Author Manuscript

NIH-PA Author Manuscript

NIH-PA Author Manuscript

and 2) the ability to assess the contributions and interactions of individual layers of multi-layered structures. Thus, multi-layered tissues like the aortic valve leaflet should reveal a distinct bending response depending on the direction of bending. Thus, flexural mechanical testing techniques are a sensitive way to explore the effects of layer contributions.

To quantify the flexural properties, we have utilized both 3-point (Engelmayr et al., 2003; Gloeckner et al., 1999; Merryman et al., 2006) and cantilever (Mirnajafi et al., 2006) loading configurations. For the aortic valve leaflet, the effective stiffness measured in the with-curvature (WC) direction is dominated by the tension in the ventricularis, with little contribution from the fibrillar collagen in the fibrosa which is not designed to support compressive loads. Conversely, when the leaflet is bent in the against-curvature (AC) direction, the fibrosa is in tension and the ventricular is in compression (Fig. 7-b). The resulting data is expressed as the bending moment (M) vs. $\Delta\kappa$, from which the effective *instantaneous* bending stiffness E can be determined using the Euler-Bernoulli equation $M = EI\,\Delta\kappa$ (Frisch-Fay, 1962), where I is the second moment of inertia. Using this technique we have found a linear M-$\Delta\kappa$ response in the belly regions (Merryman et al., 2006), in contrast to the highly non-linear in-plane tension response. Interestingly, for the commissure region E varied linearly with the deflection angle φ, indicating a consistent decrease in stiffness with increased flexure. Histological studies of the commissure region indicated that tissue buckling was a probable mechanism for decrease in E with increasing flexure. The observed change in E with flexural angle in the commissural region is a subtle aspect of valve function.

Recently, we have developed a novel, highly sensitive instrument that used an end-loaded configuration that allows for simultaneous measurement of the transmural strain distribution in the specimen center (Lam et al., submitted). Circumferential strips from porcine AV leaflets taken from the belly region (Fig. 7-a) were subjected to bidirectional flexure to the fibrosa and ventricularis layers to alternate states of in tension and compression (Fig. 7-b). The center of the specimen (approximate 2 mm in length) was marked with small ink particles which were tracked using a separate high-resolution imaging system. Transmural images were acquired at $\Delta\kappa$=0.1, 0.2, and 0.3 mm^{-1} in the AC and WC directions, where $\Delta\kappa$=0.1, 0.2, and 0.3 mm^{-1} was considered the peak change in curvature, based on in-vitro measurements (Sugimoto and Sacks, submitted). Details of the transmural strain analysis is given in (Lam et al., submitted). Briefly, from the tracked marker displacements the local deformation gradient tensor **F** determined which was decomposed into the stretch and rotation tensors, **U** and **R**, respectively to remove rigid body motion experienced by the tissue during flexure. The net stretch along each axis, Λ_i (i=1,2) was computed using $\Lambda_1=\sqrt{U_{11}^2+U_{12}^2}$ and $\Lambda_2=\sqrt{U_{22}^2+U_{12}^2}$. Thus, the location of the neutral axis, where Λ_1=1, was determined by plotting Λ_1 against the tissue thickness.

Interestingly, the Λ_1-transmural thickness relation quite linear for each flexural level in both bending directions, with Λ_1 ranging from 0.94 to 1.08 (Fig. 7-c). This suggests that the maximum tissue strains were on the order of +/−7%, which is consistent with previous work on bioprosthetic heart valves (Mirnajafi et al., 2005). Moreover, for both bending directions the neutral axis was located at 0.55–0.60 normalized tissue thickness, indicating that the fibrosa was slightly stiffer than the ventricularis in the low strain range. Of interest to layer micro-mechanics, we did not observe any slip or other evidence of shearing between layers in the transmural strain profiles. This is consistent with the highly interconnected layer microanatomy (Fig. 4). Continued work to provide insights into these mechanisms is clearly necessary to better understand native valve function.

NIH-PA Author Manuscript

NIH-PA Author Manuscript

NIH-PA Author Manuscript

4 – Constitutive models for valvular tissues

4.1 – General considerations

Advanced modeling and simulation of heart valves clearly requires sophisticated constitutive models, which are expected to account for regional variations (belly/commissure) and layer properties of valvular tissues. Moreover, they should be able to predict the stress environment of cells to address mechano-physiological questions (Huang et al., 2007). In order to frame the problem, we should consider the some important general characteristics of typical valvular mechanical responses. For example, the response to multiple planar biaxial loading protocols reveals a non-monotonic relationship between circumferential stress and strain (Fig. 8-a). Examination of the progression of the stress-strain curves with decreasing radial stress in non-equibiaxial loading protocols demonstrated that the negative circumferential strain values were due to a very strong mechanical coupling between the axes. This behavior, as well as the overall anisotropic behavior of the cusp, can be explained by the tight angular distribution of collagen fibers (Fig. 8). As one axis is loaded, the radial forces cause the fibers to rotate, which in turn cause a contraction along the circumferential axis. This effect will become more dramatic as the radial loads become larger with respect to the circumferential loads. This effect illustrates that negative strains can be generated even though the stress magnitude is the same along both axes and no buckling of the tissue is observed. Thus, radial loads are ultimately resisted by the highly circumferentially aligned fibrosa collagen fibers, whose rotation as opposed to stretch allows for large radial strains.

4.2 – Structural model

To capture this response, we utilize a meso-structural approach for constitutive modeling for planar collagenous tissues (Billiar and Sacks, 2000b; Lanir, 1983; Sacks, 2003). It is assumed that a representative volume element (RVE) can be identified that is large enough to represent the processes associated with the microstructure of the material in some average sense, yet small compared to the characteristic length scale of the microstructure, i.e. the tissue thickness. The RVE is treated as a three-dimensional continuum and it is assumed that the material can be modeled as a hyperelastic solid, so that

$$\mathbf{S}=\frac{\partial \mathrm{W}}{\partial \mathbf{E}} \tag{1}$$

where **S** and **E** are the 2nd Piola-Kirchhoff stress and Green-Lagrange strain tensors, respective, and W is the tissue strain energy density per unit volume. Within the RVE, the following assumptions are made:

1. As with other collagenous membrane tissues, valvular tissues can be idealized as a planar network of collagen fibers embedded in a compliant ground substance (i.e. the matrix).
2. The load required to straighten the collagen fiber is considered negligible compared to the load transmitted by the stretched fibers. Hence, collagen fibers transmit load only if stretched beyond the point where all the undulations have disappeared, and are assumed to be linearly elastic.
3. The fiber strain can be computed from the tensorial transformation of the global strain tensor referenced to fiber coordinates (i.e. the affine transformation assumptions).
4. The strain energy function of the tissue is the sum of the individual fiber strain energies. For the purposes of tissue-level simulations, we consider a homogenized model wherein we consider an ensemble of fibers, with varying degrees of

NIH-PA Author Manuscript

NIH-PA Author Manuscript

NIH-PA Author Manuscript

undulations, with an orientation defined by the normal vector $\hat{N} = \cos(\theta)\hat{i} + \sin(\theta)\hat{j}$ in the unloaded reference state. The resulting effective stress response was represented using $S' = c_1[\exp(c_2 E') - 1]$ where c_i are material constants, S' is the ensemble second Piola-Kirchhoff stress, and E' is the ensemble Green's strain determined using $E' = \hat{N}^T \mathbf{E}\hat{N}$. Note that for valvular tissues, it was initially more convenient to work with membrane stresses due to considerations such as variable total and layer thickness, and heterogeneous layer structure (Billiar and Sacks, 2000a). We also assume that inter-specimen variations in fiber volume fraction V_f and thickness h are negligible, so that the product hV_f can be conveniently absorbed into the material constant c_1. This model worked very well for both the native aortic and chemically modified valvular tissues (Billiar and Sacks, 2000b, 2000a).

Constitutive model that better reflects the physiologically-driven structural kinematics of collagen fibers under deformation is the next logical approach, including the use of. This includes use of fiber recruitment models (Sacks, 2003). However, fiber recruitment models are difficult to implement three dimensional soft tissues since the fiber recruitment behavior is difficult to directly obtain from conventional multi-protocol experimental protocols. There are also practical parameter optimization difficulties when utilize in multi-axial data since recruitment model parameters are non-unique and multiple combinations can fit data equally well, and thus obscure the underlying mechanisms. Thus we need appropriate theoretically-guided experiments to implement structural models for valvular tissues properly.

Our purpose was therefore to demonstrate that the constituent fibers of the left side valve leaflets can be simulated using a fiber recruitment model. As above, the strain energy measure in terms of total strain for a single fiber is given by

$$W^f(E') = \frac{K}{2}\left(\frac{E' - E_s}{1+2E_s}\right)^2. \tag{2}$$

Here, K represents the effective fiber modulus and E_s is the Green's strain in which the fiber straightens. To link the individual fiber responses to that of the ensemble, we assume that the recruitment of collagen fibers, the ensemble is represented by $D(E')$ (Lanir, 1983; Sacks, 2003), where the function D represents the probability density distribution characterizing the fiber undulation. The fiber ensemble strain energy can thus be written as

$$W'(E') = \int_0^{E'} D(x)\, W^f(E')\ dx. \tag{3}$$

Here, W' represents the strain energy developed by all fibers contributing to the load transfer at a specific angle θ within the fiber network. The resulting ensemble stress can be determined using

$$S' = \frac{\partial W'(E')}{\partial E'} = \int_0^{E'} D(x) \frac{\partial W^f(E')}{\partial E'}\ dx. \tag{4}$$

Next, integrating to the tissue level, we have

NIH-PA Author Manuscript

NIH-PA Author Manuscript

NIH-PA Author Manuscript

$$S(E)=\frac{\partial W(E)}{\partial E}=\int_{-\pi/2}^{\pi/2}R(\theta)\left\{K\int_0^{E'}D(x)\frac{E'-E_s}{(1+2E_s)^2}\,dx\right\}N\otimes N\;\theta, \tag{5}$$

where $\otimes$ indicates external multiplication so that $[\mathbf{N}\otimes\mathbf{N}]_{ij}=\mathbf{N}_i\mathbf{N}_j$ and that $R(\theta)$ is the angular distribution of the collagen fibers. Based on our architectural data for the aortic valve leaflet (Sacks et al., 1998), we utilize the fact that $R(\theta)$ can be represented by

$R(\theta)=\exp\left[\frac{-\theta^2}{2\sigma^2}\right]/(\sigma\sqrt{2\pi})$, where σ is the standard deviation.

A difficulty in implementing eqn. 5 in the homogenized tissue constitutive model is the determination of the fiber recruitment function D. In particular, the tissue response should exhibit a distinct upper bound strain, E_{ub}, which represents the strain wherein all collagen fibers have been fully recruited. At the tissue level, full recruitment is characterized by a constant stiffness for $E_{ens}\geq E_{ub}$. Thus, the D must be defined over a finite Green's strain range $E_{ens}\in[0, E_{ub}]$, and 0 otherwise, with $\int_0^{E_{ub}}D(x)dx=1$. It can be shown that under equibiaxial strain conditions ($E_{11}=E_{22}$, $E_{12}=S_{12}=0$), the fiber ensemble stress-strain law can be obtained directly from the biaxial mechanical data using $S'=S_{11}+S_{22}$ (Sacks, 2003). From the S′-E′ response curve and eqn. 3, the effective fiber stiffness K and D can be determined. For D, we utilized the following modified beta function

$$D(x)=\frac{x^{\gamma-1}(1-x)^{\delta-1}\Gamma(\gamma+\delta)}{\Gamma(\gamma)\Gamma(\delta)}\ \text{for}\ x\in[0,E_{ub}],\ \ 0\ \text{otherwise}, \tag{6}$$

where γ and δ are constants related to the distribution mean $\mu=\gamma/(\gamma+\delta)$ and variance $\sigma=\sqrt{(\gamma\delta)/\left[(\gamma+\delta)^2(\gamma+\delta+1)\right]}$.

Experimentally, the E_{ub} is determined by finding the onset of constant stiffness from the S′-E′ response curve, best determined from strain value where the tangent modulus plateaus (Figs. 9-a,b). To determine the ensemble model parameters K, μ, and σ, eqn.4 was fit to the to S′-E′ data using Marquardt-Levenberg non-linear least squares algorithm (Press et al., 1988). Using the post-transition tangent modulus value (equivalent to the maximum tangent modulus) was used as an initial estimate to the collagen fiber elastic modulus K. When applied to the native MVAL, MVPL, and AV The recruitment model was found to fit the data quite well, with an r2 ≅ 0.99. AVL was found to have the Eub = 0.3013 ± 0.0323, in comparison with MVAL (0.2692 ± 0.0487) and MVPL (0.2473 ± 0.01181). Moreover, the model predicted the very similar average K values for each valve leaflet type (mean ± sem, n=6 each): MVAL 123.443 ± 3.324 MPa, MVPL = 124.114 ± 7.830 MPa, and AV=101.220 ± 6.030 MPa. It is interesting to note that these values are very similar to the 95.5 MPa measured using SAXS for the MVAL (Liao et al., 2007).

In addition to greater structural realism, the recruitment model can also perform better in stress overload situations. For example, both the exponential model and the recruitment model were fitted to the same equi-biaxial strain data (Fig. 9-c,d). We then simulated the trend beyond the used data range and examined the predicted trend with the 10 real datum points. As anticipated, the exponential model predicted a continuous increase in tensile modulus with increased strain, whereas the fiber recruitment model provided accurately predicted the linear stress-strain relationship beyond the data range (Figure 7b). This result indicates the need for realistic

NIH-PA Author Manuscript

NIH-PA Author Manuscript

NIH-PA Author Manuscript

constitutive models capable of prediction outside the range used to define the model, especially in situations where stress-overloads need to be accurately predicted.

4.3 – 3D stress model

All existing constitutive models for heart valve leaflet tissues assume either a uniform transmural stress distribution or utilize a membrane tension formulation. Both approaches ignore layer specific mechanical contributions and the implicit non-uniformity of the transmural stress distribution. Both the structural and mechanical data, especially the observation of the extensive network of inter-layer connections (Fig. 4-b) and identical strains under biaxial loading (Stella and Sacks, 2007) and the continuous transmural strain distribution (Fig. 7) suggest that the layers are tightly bonded. More importantly, they call into question the functional role of the spongiosa and whether it is a functional layer. Traditional thinking suggests that the spongiosa enables local movement and shearing between the fibrosa and ventricularis layers during dynamic loading due to its loose organization (Talman, 1996;Talman and Boughner, 2001,1995). Instead, we view the spongiosa from a functional perspective: as an interior surface specialization of the fibrosa and ventricularis layers that strongly resists delamination through extensive collagen fiber inter-connections.

To develop an actual 3D stress model that accounts for layer specific contributions, we conducted novel studies to quantify the biaxial mechanical behavior of the two structurally distinct, load bearing aortic valve (AV) leaflet layers: the fibrosa and ventricularis (Stella and Sacks, 2007). For a bilayer tissue configuration, we utilized individual layers in their separated, stress free reference configuration and reconstruct the 3D stresses. We modified the equation 5 to include the separate contributions of both layers (Stella and Sacks, 2007), accounting for the different reference states of each layer (Stella and Sacks, 2007). Key results demonstrated that the fibrosa layer dominated the circumferential direction response (Fig. 10). Interestingly, the ventricularis experienced approximately twice the stress level at full physiological deformations. Moreover, the model also indicated that the ventricularis does not contribute to the radial component until a radial stretch of ~1.4. Clearly, layer micromechanics play a substantial role in valve leaflet function.

5 – Cellular function

5.1– Introduction

Within the three layers of the leaflet tissue, there resides a heterogenic population of interstitial cells (Filip et al., 1986; Messier et al., 1994; Mulholland and Gotlieb, 1996; Taylor et al., 2003). The heterogeneity of the interstitial cells is made up of fibroblasts, smooth muscle cells, and myofibroblasts, which have characteristics of both fibroblasts and smooth muscle cells. Studies of the interstitial cell population in both human and porcine subjects have revealed that the interstitial cell population was not localized to any one region or layer of the leaflet, but was present throughout the tissue (Bairati and DeBiasi, 1981; Merryman et al., 2006). The leaflets of all four HVs are also sheathed by single layer valvular endothelial cells (VECs), shown to be morphologically different from aortic ECs (Butcher and Nerem, 2004; Butcher et al., 2004). Additionally, VECs are aligned with the collagen architecture of the valve, which is circumferentially oriented (Deck, 1986). The VECs are believed to regulate vascular tone, inflammation, thrombosis, and remodeling, and their dysfunction has been linked with multiple disorders (Leask et al., 2003). Primarily, release of cytokines has been shown to cause changes in interstitial cell structure and function (Davies, 1997; Davies and Tripathi, 1993). It has also been speculated that there exists some physical communication between the VECs and VICS. However, to date no direct junctions have been observed between the two cell populations (Filip et al., 1986).

NIH-PA Author Manuscript

NIH-PA Author Manuscript

NIH-PA Author Manuscript

Interest in the myofibroblast cells (typically referred to as VICs) has grown in recent years, as they are believed to be critically important in valve pathophysiology. Primarily, VICs serve to maintain the structural integrity of the leaflet tissue by remodeling via protein synthesis and enzymatic degradation (e.g. MMPs). Their phenotype (which ranges from fibroblast-like to myo-like) is believed to be plastic and reversible, as VICs of normal, healthy valves were quiescent while in developing, diseased, and remodeling valves, the VICs were activated and contractile (Rabkin-Aikawa et al., 2004; Rabkin et al., 2002). While their dualistic nature is not fully understood, the VIC's multifunctionality may be used for cell-cell communication, tissue remodeling, wound healing, and contraction (Mulholland and Gotlieb, 1996). Further, it is believed that when the phenotype of the resident VIC population is myo-like, the cells are actively remodeling the ECM. This indicates that the VIC phenotypic state at any given time is likely related to the current remodeling demands of the tissue (Rabkin et al., 2002).

5.2 – VIC micromechanical environment

While it is known that AVICs can respond to mechanical stimuli in-vitro, the level of in-vivo AVIC deformation and its relation to local collagen fiber reorientation during the cardiac cycle remain unknown. To elucidate the micromechanics of the valve leaflets to increasing strain and the VIC micromechanical environment, AV leaflets were obtained, dissected from the aortic root, and subjected to a single extension of 0, 10, or 20% strain and fixed with either 2.5% Grade I or Grade II (EM grade) glutaraldehyde (Sigma Aldrich, St. Louis, MO) for 60 min in their strained state. Afterwards, the strips were either analyzed by small angle light scattering (SALS) (Sacks et al., 1997) to determine the change in collagen orientation with increasing strain, or imaged by transmission electron microscopy (TEM) to determine changes in cellular deformations. From the SALS measurements, we determined the normalized orientation index (Gilbert et al., 2006), a percentile scale of fiber orientation. From the TEM images, the orthogonal major and minor axes of the cell and nucleus were measured (SigmaScan, SYSTAT) and used to calculate aspect ratios as reported previously for AVICs fixed under increasing pressure (Huang et al., 2007; Kim et al., 2008).

As found previously (Sacks et al., 1997), increasing diastolic pressure induced increased NOI increased appreciably with increasing strain (Figure 11-a). Note that that there is no change in NOI from 10 to 20% strain demonstrate that 10% strain is sufficient to largely orient the collagen fibers. Since the myofibroblast nucleus makes up a sizeable portion of the cell volume, we found the cell and nucleus aspect ratio increase together with increasing strain (Figs. 11b,c). The nuclear aspect ratios were significantly greater ($p<0.05$) for the both the cell and nucleus at 20% compared to 0 and 10%. This finding also demonstrates that the nucleus is indeed a reliable cellular strain gage.

Based on these studies, we quantified VIC deformation under physiological loading conditions using porcine AV glutaraldehyde fixed under 0 to 90 mmHg transvalvular pressures. The resulting change in nuclear aspect ratio (NAR) was used as an index of overall cellular strain, and dependencies on spatial location and pressure loading levels quantified. Local collagen fiber alignment in the same valves was also quantified using small angle light scattering (SALS). When the VIC nuclear aspect ratios were plotted against normalized leaflet thickness, TVP level was found to have a significant effect on NAR values (Fig. 11-d). At zero mmHg the AVIC NAR maintained a constant transmural value of ~1.8. In the fibrosa layer (normalized thickness range from ~0.4 to 1), the AVIC NAR at 4 mmHg slightly increased. Under peak physiological transvalvular pressure (90 mmHg), the AVIC NAR were not only substantially greater than at low-pressure levels, but also demonstrated substantial transmural variations. In particular, the NAR exhibited greater increases in the fibrosa layer (~4.8 compared to ~3.0 for the ventricularis layer), which were statistically larger than both the corresponding 90 mmHg

NIH-PA Author Manuscript

NIH-PA Author Manuscript

NIH-PA Author Manuscript

ventricularis and lower pressure NAR values ($p < 0.05$). This result indicated additional micromechanical and fiber-compaction effects occur at high pressure levels.

5.3 – VIC mechanical behavior

VICs are phenotypically plastic as they transdifferentiate into myofibroblasts during times of valve development, disease, and remodeling (Rabkin-Aikawa et al., 2004). One major indicator of VIC phenotype is the level of smooth muscle α-actin (SMA), which should dramatically affect cell stiffness. To begin to address this question, we have isolated ovine VICs from the four heart valves and subjected them to micropipette aspiration to assess cellular stiffness, and cytoskeletal composition and collagen biosynthesis were quantified using surrogates smooth muscle α-actin (SMA) (Merryman et al., 2006). Results revealed that VICs from the aortic and mitral valves were significantly stiffer ($p<0.001$) than the pulmonary and tricuspid VICs (Fig. 12-a). Additionally, left side isolated VICs contained significantly more ($p<0.001$) SMA and Hsp47 than the right side VICs. Mean VIC stiffness correlated well ($r=0.973$) with TVP; SMA and Hsp47 also correlated well ($r=0.996$) with one another. Moreover, assays were repeated for VICs in situ, and as with the in vitro results, the left side VIC protein levels were significantly greater ($p<0.05$).

However, the mechanical properties of VICs have been measured under essentially quasi-static time frames, including both by micropipette (Merryman et al., 2006) and atomic force microscopy (Merryman et al., 2007). However, due to the rapid loading time of the AV leaflets during closure (~0.05 s), time-dependent effects may play a role in VIC deformation during physiological function. Recently, we explored AVIC viscoelastic behavior using the micropipette aspiration technique (Merryman et al., in press). We then modeled the resulting time-length data over the 100 sec test period using a standard linear solid (SLS) model which included Boltzmann superposition (Fig. 12-b). To quantify the degree of creep and stress relaxation during physiological timescales, simulations of micropipette aspiration were preformed with a valve loading time of 0.05 s and a full valve closure time of 0.3 s. The 0.05 s loading simulations suggest that, during valve closure, AVICs act elastically. During diastole, simulations revealed creep (4.65%) and stress relaxation (4.39%) over the 0.3 s physiological timescale. Simulations also indicated that if Boltzmann superposition was not used in parameter estimation, as in much of the micropipette literature, creep and stress relaxation predicted values were nearly doubled (7.92% and 7.35%, respectively). We conclude that while AVIC viscoelastic effects are negligible during valve closure, they likely contribute to the deformation time-history of AVIC deformation during diastole.

The above studies were conducted on isolated cells, while the role of VIC and extracellular matrix (ECM) interactions are not well understood. For example, the distinct differences in the composition and structure of the AV leaflet layers (fibrosa and ventricularis) have been shown to influence mechanical properties (Stella and Sacks, 2007). Our ability to measure the effects of changes in cellular stiffness in the dense collagenous valvular leaflets (Merryman et al., 2006) offers a unique opportunity to explore the in-situ VIC stiffness and local VIC-ECM mechanical interactions. To better determine the in-situ VIC stiffness, a multi-scale finite element model approach was developed based on our simulations of our flexural stiffness experiment were used to develop effective layer dependent mechanical properties (Fig 13). The bi-layer finite element model described was utilized as a macro scale model providing driving mechanical conditions to the micro cell-based model. The adopted approach is rooted in the mapping of micro region boundary deformations from the macro scale results. A two-dimensional plane stress finite model representing the 100 μm × 100 μm square section of tissue in the fibrosa was developed (Fig. 13). Based on available histological data presented above, cell dimensions were assumed to be 6 μm × 3.3 μm with the micro scale model containing 37 cells distributed in an uniform pattern simulating measured densities. The micro

NIH-PA Author Manuscript

NIH-PA Author Manuscript

NIH-PA Author Manuscript

model ECM was modeled using a neo-Hookean material to match the assumption associated with the tissue level model, with the cell regions were modeled as a linear isotropic elastic material. Nodal displacements on the exterior boundary of the cell scale model are defined from interpolation of the displacement field of the deformed tissue scale model.

Macro-model simulation results indicated maximum principal strain of less than 5% for curvatures up to 0.12 mm^{-1}, a condition which supports the neo-Hookean material assumption. Further, macro model effectively predicted the nearly linear response observed by flexural testing (Fig. 13-a) (Merryman et al., 2006). Given the assumption that the fibrosa and ventricularis layer properties are dissimilar in a contracted state under AC conditions, the estimated fibrosa layer neo-Hookean modulus was 2.3 times greater than ventricularis layer. For this state, the ventricularis layer was parameterized with normal basal tonus properties (70 kPa) in combination with a fibrosa layer shear modulus of 160 kPa. The effect of basal tonus was to raise the base tissue response from 40 to 70 kPa in both layers.

However, at the micro-scale we determined that, as an independent mechanism, increases in cell stiffness alone cannot lead to a significant increases gross tissue stiffness. This property further suggests that cell contraction precipitates an increase in surrounding ECM. With respect to leaflet mechanical response in a low strain environment, cell contraction serves as a contributing mechanism. In contrast to the fiber dominated response to transvalvular pressure during valve closure, during valve opening the leaflets are highly compliant operating in a flexural mode of deformation. In this flexure dominated environment, the nature of cell-ECM interaction under contractile states may play an important role in regulating AVIC mechanobiological responses during normal valve function. Our present work also showed the potential layer specific effects the contractility of the AVIC population can have, particularly in the oft-diseased fibrosa layer of the AV. Pathologic and etiologic data indicate that nearly all cases of degenerative valve disease initiate and propagate from the fibrosa layer.

6 – Summary and Future trends

Growth and remodeling of valvular tissues

Biomechanics is ideally suited toward the study of valve function as it takes an “integrated” approach rather than a reductionist approach common to the biological sciences. This will be important not only for understanding basic valve pathologies, but also in related valvular issues never explored. For example, although other cardiovascular tissues, such as myocardium and aorta, have been shown to remodel when exposed to chronic changes in hemodynamic stresses, it has been ardently debated whether heart valves have the capacity to remodel in a non-pathological state

Perhaps the most interesting ways to look at valvular remodeling is the remodeling of clinical pulmonary-to-aortic valve transplants. Rabkin-Aikawa et al. (Rabkin-Aikawa et al., 2004) studied the pathologic features, cellular phenotypes, and matrix remodeling of clinical pulmonary-to-aortic valve transplants functioning up to 6 years. Autografts were found to be near-normal trilaminar cuspal structure and collagen architecture and viable valvular interstitial and endothelial cells throughout the time course. In contrast, cusps of homografts used to replace the pulmonary valves in the same patients were devitalized. Collagen content in autografts was comparable with that of normal valves and was higher than that seen in homograft valves. However, autograft walls were damaged, with granulation tissue (early) and scarring, with focal loss of normal smooth muscle cells, elastin, and collagen (late). Thus, the structure of pulmonary valves transplanted to the systemic circulation evolved toward that of normal aortic valves, with key processes including onset of a systemic endothelial cell phenotype and reversible plasticity of fibroblast-like valvular interstitial cells to myofibroblasts. In a related study, Aikawa et al. (Aikawa et al., 2006) performed quantitative

NIH-PA Author Manuscript

NIH-PA Author Manuscript

NIH-PA Author Manuscript

histological assessment of 91 human semilunar valves obtained from fetuses at 14 to 19 and 20 to 39 weeks' gestation; neonates minutes to 30 days old; children aged 2 to 16 years; and adults. They concluded that fetal valves possess a dynamic/adaptive structure and contain cells with an activated/immature phenotype. During postnatal life, activated cells gradually become quiescent, whereas collagen matures, which suggests a progressive, environmentally mediated adaptation

Another model of valvular remodeling is pregnancy, which produces dramatic hemodynamic and hormonal changes. Wells and Moeller have recently shown that (Wells and Moeller, 2008) for the first time, physiological remodeling of mature heart valve leaflets in a non-pathological state. Adaptive remodeling of heart valve leaflets during pregnancy involves dramatic changes in leaflet mechanical properties, dimensions, and composition, and these changes appear to be valve-dependent. These results have significant implications for heart valve tissue engineering. Understanding the mechanical and hormonal triggers of this remodeling will aid in directing the proper structural/functional development of tissue engineered leaflet tissues. These results also imply that engineered heart valves should *maintain* an implicit capacity for remodeling post-implantation.

The development of aortic valve problems in patients with LVADs has been reported previously (Park et al., 2004). Left ventricular assist device (LVAD) is a pump surgically connected to the heart and aorta in order to boost systemic blood flow (Rose et al., 2001). Aortic dysfunction in LVAD patients can develop within 6–12 months of LVAD implantation. It is estimated that approximately 50% of patients with pulsatile LVADs develop aortic insufficiency (AI) or aortic stenosis (AS) (Park et al., 2004). One institution reports routinely using ultrasound imaging to evaluate patients on VAD support for more than six months, finding that 50% of patients developed inappropriately increased rates and flows and are found to have mild to moderate degrees of native AI (Samuels et al., 2001). Insidious onset and progression of AI may also occur for undefined reasons such as (i) leaflet elongation, (ii) sinotubular dilatation, (iii) annular dilatation or (iv) any combination of the above. LVAD-induced structural abnormalities in the native aortic valve have been found in a significant number of LVAD patients as well, in particular the observation of commissural fusion. Aortic commissural fusion is a remodeling process in which fibrous tissue is deposited at the commissures of the coapted leaflets, adhering them together and preventing complete opening. Fusion can occur in one, two or all three of the cusps and usually covers a total of several mm of commissural length summed over all leaflets (Rose et al., 2000; Connelly et al., 2003). Recent studies have linked LVAD use to higher transvalvular pressures across the aortic valve (Travis et al., 2007; Zamarripa Garcia et al., 2008), and have found that strain in the valve leaflets is increased in LVAD patients, particularly under series flow conditions (Enriquez et al., 2008). These findings suggest that the development of aortic fusion is related to the increase in mechanical stress and strain in the leaflets, as they are subjected to higher transvalvular pressures for a longer percentage of the cardiac cycle than under normal flow conditions. Further investigation into LVAD-induced remodeling and dysfunction of the aortic valve are warranted.

Computational approaches to valve function

In the authors' opinion, we are now entering a level of bioengineering knowledge of valvular function wherein computational approaches can begin to realistically be applied. For example, recent work from the Einstein et al. on dynamic modeling (Einstein et al., 2004; Einstein et al., 2005) simulated early acoustic detection of changes in mitral valve properties, which may lead to the better management of mitral valve disease. To model the transient vibrations of the mitral valve apparatus bathed in a blood medium, they constructed a dynamic nonlinear fluid-coupled finite element model of the valve leaflets and chordae tendinae. The gross movement and small-

NIH-PA Author Manuscript

NIH-PA Author Manuscript

NIH-PA Author Manuscript

scale acoustic vibrations of the valvular structures result from the application of physiologic pressure loads. Material changes that preserved the anisotropy of the valve leaflets were found to preserve valvular function. By contrast, material changes that altered the anisotropy of the valve were found to profoundly alter valvular function. These changes were manifest in the acoustic signatures of the valve closure sounds. Abnormally, stiffened valves closed more slowly and were accompanied by lower peak frequencies.

Recent work by Driessen et al. (Driessen et al., 2003; Driessen et al., 2005) developed a finite-element (FE) model to relate changes in collagen fiber content and orientation to the mechanical loading condition within the engineered heart valve construct. They hypothesized that collagen fibers aligned with principal strain directions and that collagen content increased with the fiber stretch. The results indicate that the computed preferred fiber directions run from commissure to commissure and show a resemblance to experimental data from native aortic heart valves. These models represent only a first step in developing physiologically realistic models of heart valve function. In particular there is a need for thorough experimental validation and true dynamic models that couple tissue (solid) and blood (fluid). For example, Kim et al. have developed (Kim et al., 2007; Kim et al., 2006) have shown for pericardial bioprosthetic heart valves that In addition, the present simulation also demonstrated the importance of including the bending component together with the in-plane material behavior of the leaflets towards physiologically realistic deformation of the leaflets. Moreover, dynamic simulations with experimentally determined leaflet material specification can be potentially used to modify the valve towards an optimal design to minimize regions of stress concentration and structural failure.

Surgical replacement of diseased heart valves by mechanical and tissue valve substitutes is now commonplace and enhances survival and quality of life for many patients. However, repairs of congenital deformities require very small valve sizes that are simply not commercially available. Further, in pediatric applications growth of the replacement valve is essential to eliminate the need for reoperations as the patient grows. There are a variety of devices available for replacement of cardiac valves, but all current devices have significant limitations that result in a continuing risk for morbidity and mortality (Schoen and Levy, 1999). The ultimate heart valve replacement is characterized as non-obstructive, non-thrombogenic living tissue valve substitute that lasts the lifetime of the patient, provides ongoing remodeling and repair of cumulative injury and potentially grows with the recipient is an important goal. Such a valve would be particularly useful in the treatment of the approximately 20,000 children with congenital heart disease born in the United States each year and especially those with valvular disease. In this population the anticoagulation required with mechanical valves is particularly dangerous and tissue valve substitutes undergo accelerated calcification. Moreover, the placement of oversized valves extra-anatomically in the right ventricular outflow necessitates multiple subsequent surgeries for these children as valves and conduit devices repeatedly become stenosed over time. Thus, a fundamental problem inherent to the use of existing mechanical and biological prostheses in the pediatric population is their failure to grow, repair and remodel. Regardless of the design specifics of current prosthetic valve devices, none offers any potential for growth, and therefore pediatric patients requiring valve replacement will require reoperations to place larger devices to accommodate the growth of the patient (Kirklin et al., 1993).

For example, it has been reported the gradual development of a tri-layered structure, including variations in collagen, GAG, and elastin, after 15–20 weeks post implantation (Rabkin et al., 2002). Yet, we do not know if these layers are functionally equivalent to the native valve, and even what mechanisms guide their formation in-vivo, nor do we have no knowledge of the anisotropic mechanical properties of TEHV leaflet tissue, and how well these compare with the native PV (Sacks et al., 2009). In the principals of Functional Tissue Engineering (Butler

NIH-PA Author Manuscript

NIH-PA Author Manuscript

NIH-PA Author Manuscript

et al., 2000), it is stated that there a need to establish the minimal functional parameters necessary to produce tissue equivalents. For heart valves, this includes quantification of the anisotropic mechanical properties of TEHV leaflet tissue, which can only be achieved thru multi-axial testing to determine if the developing tissue is a suitable valve replacement. Further, the degree of cellular function and similarity to the native valve has yet to be determined. Yet, despite the fundamental nature of these requirements, we currently have no knowledge of the TEHV functional similarity at the tissue and cellular levels to the native PV, which will ultimately dictate functionality and long-term durability (Sacks et al., 2009).

Ultimately, we would like to connect the organ-scale simulations to evaluate our understanding of AVIC mechano-transduction, it would be beneficial to develop an AVIC phenotypic/biosynthetic model linked to organ-level deformations. In the AVL, transvalvular pressures (TVPs) above ~5 mmHg predominately result in ECM compaction as the collagen fibers become uncrimped and taut. From this ECM compaction, significant AVIC nucleus aspect ratio has been observed with increasing pressures (Fig. 13). Even a phenomenological model could thus simulate the AVIC population with mechanical inputs (quantified by the deformation of the AVIC nuclei) and cytokine activity. It could then be possible to predict the phenotypic and biosynthetic response of AVICs after repeated loading cycles.

Acknowledgments

Funding for the work presented in this paper was generously provide by NIH R01 HL68816, HL63026 HL089750, HL071814, HL073021, HL520009, EB003392 T32 Pre-doctoral Training Grant, an AHA Established Investigator Award to MSS, and an AHA PA-DE Pre-doctoral Fellowship to WDM. The authors would also like to acknowledge Sarah Vigmostad and K.B. Chandran of the University of Iowa for the material provided in Figure 3.

NOMENCLATURE

AV
: Aortic valve

AC
: when referred to flexure, the direction against the natural curvature of the leaflet

AVEC
: aortic valve endothelial cell

AVIC
: aortic valve interstitial cell

CFD
: computational fluid dynamic (modeling)

Δκ
: Change in curvature in flexure

E
: the effective stiffness in flexure

EC
: endothelial cell

ECM
: extracellular matrix

GAG
: glycosaminoglycans

NIH-PA Author Manuscript

NIH-PA Author Manuscript

NIH-PA Author Manuscript

HSP47
heat shock protein 47

I
second moment of inertia

M
Applied bending moment

MV
mitral valve

MVAL
mitral valve anterior leaflet

MVPL
mitral valve posterior leaflet

PV
Pulmonary valve

SMA
smooth muscle actin (intracellular)

TEHV
tissue engineered heart valve

TV
Tricuspid valve

TVP
transvalvular pressure

VIC
valvular interstitial cell

WC
when referred to flexure, the direction with the natural curvature of the leaflet

References

1. Adamczyk MM, Vesely I. Characteristics of compressive strains in porcine aortic valves cusps. J Heart Valve Dis 2002;11(1):75–83. [PubMed: 11843509]
2. Aikawa E, Whittaker P, Farber M, Mendelson K, Padera RF, Aikawa M, Schoen FJ. Human semilunar cardiac valve remodeling by activated cells from fetus to adult: implications for postnatal adaptation, pathology, and tissue engineering. Circulation 2006;113(10):1344–52. [PubMed: 16534030]
3. Arts T, Meerbaum S, Reneman R, Corday E. Stresses in the closed mitral valve: a model study. J Biomech 1983;16(7):539–47. [PubMed: 6619171]
4. Bairati A, DeBiasi S. Presence of a smooth muscle system in aortic valve leaflets. Anatomy and Embryology 1981;161(3):329–40. [PubMed: 7187826]
5. Bellhouse BJ, Bellhouse FH. Fluid mechanics of the mitral valve. Nature 1969;224:615–618. [PubMed: 5346605]
6. Billiar KL, Sacks MS. Biaxial mechanical properties of the native and glutaraldehyde-treated aortic valve cusp: Part II--A structural constitutive model. Journal of Biomechanical Engineering 2000b;122(4):327–35. [PubMed: 11036555]

NIH-PA Author Manuscript

NIH-PA Author Manuscript

NIH-PA Author Manuscript

7. Billiar KL, Sacks MS. Biaxial mechanical properties of the natural and glutaraldehyde treated aortic valve cusp--Part I: Experimental results. Journal of Biomechanical Engineering 2000a;122(1):23–30. [PubMed: 10790826]
8. Broom, N.; Christie, GW. The Structure/Function Relationship of Fresh and Gluteraldehyde-Fixed Aortic Valve Leaflets. In: Cohn, LH.; Gallucci, V., editors. Cardiac Bioprosthesis. New York: Yorke Medical Books; 1982. p. 477-491.
9. Brossollet LJ, Vito RP. An alternate formulation of blood vessel mechanics and the meaning of the in vivo property. J Biomech 1995;28(6):679–87. [PubMed: 7601867]
10. Butcher JT, Nerem RM. Porcine aortic valve interstitial cells in three-dimensional culture: comparison of phenotype with aortic smooth muscle cells. J Heart Valve Dis 2004;13(3):478–85. [PubMed: 15222296]discussion 485–6
11. Butcher JT, Penrod AM, Garcia AJ, Nerem RM. Unique morphology and focal adhesion development of valvular endothelial cells in static and fluid flow environments. Arterioscler Thromb Vasc Biol 2004;24(8):1429–34. [PubMed: 15117733]
12. Butler DL, Goldstein SA, Guilak F. Functional tissue engineering: the role of biomechanics. J Biomech Eng 2000;122(6):570–5. [PubMed: 11192376]
13. Carew EO, Barber JE, Vesely I. Role of preconditioning and recovery time in repeated testing of aortic valve tissues: validation through quasilinear viscoelastic theory. Ann Biomed Eng 2000;28(9): 1093–100. [PubMed: 11132193]
14. Carew EO, Talman EA, Boughner DR, Vesely I. Quasi-Linear Viscoelastic theory applied to internal shearing of porcine aortic valve leaflets. J Biomech Eng 1999;121(4):386–92. [PubMed: 10464692]
15. Christie GW. Anatomy of aortic heart valve leaflets: the influence of glutaraldehyde fixation on function. European Journal of Cardio-Thoracic Surgery 1992;6:S25–S33. [PubMed: 1389275]
16. Christie GW, Barratt-Boyes BG. Age-Dependent Changes in the Radial Stretch of Human Aortic Valve Leaflets Determined by Biaxial Stretching. Annals of Thoracic Surgery 1995;60:S156–159. [PubMed: 7646149]
17. Dagum P, Green GR, Nistal FJ, Daughters GT, Timek TA, Foppiano LE, Bolger AF, Ingels NB Jr, Miller DC. Deformational dynamics of the aortic root: modes and physiologic determinants. Circulation 1999;100(19 Suppl):II54–62. [PubMed: 10567279]
18. Davies PF. Mechanisms involved in endothelial responses to hemodynamic forces. Atherosclerosis 1997;131 Suppl:S15–7. [PubMed: 9253470]
19. Davies PF, Tripathi SC. Mechanical stress mechanisms and the cell. An endothelial paradigm. Circ Res 1993;72(2):239–45. [PubMed: 8418981]
20. De Hart J, Peters GW, Schreurs PJ, Baaijens FP. A three-dimensional computational analysis of fluid-structure interaction in the aortic valve. J Biomech 2003;36(1):103–12. [PubMed: 12485644]
21. De Hart J, Peters GW, Schreurs PJ, Baaijens FP. A two-dimensional fluid-structure interaction model of the aortic valve. J Biomech 2000;33(9):1079–88. [PubMed: 10854880]
22. Deck JD. Endothelial cell orientation on aortic valve leaflets. Cardiovasc Res 1986;20(10):760–7. [PubMed: 3791342]
23. Driessen NJ, Boerboom RA, Huyghe JM, Bouten CV, Baaijens FP. Computational analyses of mechanically induced collagen fiber remodeling in the aortic heart valve. J Biomech Eng 2003;125 (4):549–57. [PubMed: 12968580]
24. Driessen NJ, Bouten CV, Baaijens FP. Improved prediction of the collagen fiber architecture in the aortic heart valve. J Biomech Eng 2005;127(2):329–36. [PubMed: 15971711]
25. Duran CM, Gunning AJ. The vascularization of the heart valves: a comparative study. Cardiovasc Res 1968;2(3):290–6. [PubMed: 5670736]
26. Eckert C, Zubiate B, Gorman JH, Gorman RC, Sacks MS. In-vivo dynamic deformation of the mitral valve annulus. Annals of Biomedical Engineering. submitted
27. Einstein DR, Kunzelman KS, Reinhall PG, Cochran RP, Nicosia MA. Haemodynamic determinants of the mitral valve closure sound: a finite element study. Med Biol Eng Comput 2004;42(6):832–46. [PubMed: 15587476]
28. Einstein DR, Kunzelman KS, Reinhall PG, Nicosia MA, Cochran RP. The relationship of normal and abnormal microstructural proliferation to the mitral valve closure sound. J Biomech Eng 2005;127 (1):134–47. [PubMed: 15868796]

NIH-PA Author Manuscript

NIH-PA Author Manuscript

NIH-PA Author Manuscript

29. Engelmayr GC Jr, Hildebrand DK, Sutherland FW, Mayer JE Jr, Sacks MS. A novel bioreactor for the dynamic flexural stimulation of tissue engineered heart valve biomaterials. Biomaterials 2003;24 (14):2523–32. [PubMed: 12695079]
30. Filip DA, Radu A, Simionescu M. Interstitial cells of the heart valve possess characteristics similar to smooth muscle cells. Circulation Research 1986;59(3):310–320. [PubMed: 3769149]
31. Frisch-Fay, R. Flexible bars. Washington, DC: Butterworths; 1962.
32. Fung, YC. Biomechanics: Mechanical Properties of Living Tissues. New York: Springer Verlag; 1993.
33. Gilbert TW, Sacks MS, Grashow JS, Woo SL, Badylak SF, Chancellor MB. Fiber kinematics of small intestinal submucosa under biaxial and uniaxial stretch. J Biomech Eng 2006;128(6):890–8. [PubMed: 17154691]
34. Gloeckner DC, Billiar KL, Sacks MS. Effects of mechanical fatigue on the bending properties of the porcine bioprosthetic heart valve. Asaio J 1999;45(1):59–63. [PubMed: 9952009]
35. Gorman JH 3rd, Gupta KB, Streicher JT, Gorman RC, Jackson BM, Ratcliffe MB, Bogen DK, Edmunds LH Jr. Dynamic three-dimensional imaging of the mitral valve and left ventricle by rapid sonomicrometry array localization. J Thorac Cardiovasc Surg 1996;112(3):712–26. [PubMed: 8800160]
36. Gorman JH 3rd, Jackson BM, Enomoto Y, Gorman RC. The effect of regional ischemia on mitral valve annular saddle shape. Ann Thorac Surg 2004;77(2):544–8. [PubMed: 14759435]
37. Grande-Allen KJ, Calabro A, Gupta V, Wight TN, Hascall VC, Vesely I. Glycosaminoglycans and proteoglycans in normal mitral valve leaflets and chordae: association with regions of tensile and compressive loading. Glycobiology 2004;14(7):621–33. [PubMed: 15044391]
38. Grande KJ, Cochran RP, Reinhall PG, Kunzelman KS. Stress variations in the human aortic root and valve: the role of anatomic asymmetry. Ann Biomed Eng 1998;26(4):534–45. [PubMed: 9662146]
39. Grashow, J. Bioengineering. Pittsburgh: University of Pittsburgh; 2005. Evaluation of the biaxial mechanical properties of the mitral valve leaflet under physiological loading conditions . Masters: 187
40. Grashow JS, Sacks MS, Liao J, Yoganathan AP. Planar biaxial creep and stress relaxation of the mitral valve anterior leaflet. Ann Biomed Eng 2006a;34(10):1509–18. [PubMed: 17016761]
41. Grashow JS, Yoganathan AP, Sacks MS. Biaxial stress-stretch behavior of the mitral valve anterior leaflet at physiologic strain rates. Ann Biomed Eng 2006b;34(2):315–25. [PubMed: 16450193]
42. Guyton, AC. Textbook of Medical Physiology. Philadelphia: W.B. Saunders Company; 1976.
43. Hartiala JJ, Mostbeck GH, Foster E, Fujita N, Dulce MC, Chazouilleres AF, Higgins CB. Velocity-encoded cine MRI in the evaluation of left ventricular diastolic function: measurement of mitral valve and pulmonary vein flow velocities and flow volume across the mitral valve. Am Heart J 1993;125 (4):1054–66. [PubMed: 8465728]
44. He Z, Ritchie J, Grashow JS, Sacks MS, Yoganathan AP. In vitro dynamic strain behavior of the mitral valve posterior leaflet. J Biomech Eng 2005;127(3):504–11. [PubMed: 16060357]
45. He Z, Sacks MS, Baijens L, Wanant S, Shah P, Yoganathan AP. Effects of papillary muscle position on in-vitro dynamic strain on the porcine mitral valve. J Heart Valve Dis 2003;12(4):488–94. [PubMed: 12918852]
46. Hilbert SL, Barrick MK, Ferrans VJ. Porcine aortic valve bioprostheses: A morphologic comparison of the effects of fixation pressure. Journal of Biomedical Materials Research 1990;24:773–787. [PubMed: 2113925]
47. Hilbert SL V, Ferrans J, Swanson WM. Optical methods for the nondestructive evaluation of collagen morphology in bioprosthetic heart valves. Journal of Biomedical Materials Research 1986;20:1411–1421. [PubMed: 3782189]
48. Huang HY, Liao J, Sacks MS. In-situ deformation of the aortic valve interstitial cell nucleus under diastolic loading. J Biomech Eng 2007;129(6):880. [PubMed: 18067392]
49. Iyengar AKS, Sugimoto H, Smith DB, Sacks MS. Dynamic in vitro quantification of bioprosthetic heart valve leaflet motion using structured light projection. Ann Biomed Eng 2001;29(11):963–73. [PubMed: 11791679]
50. Joyce EM, Liao J, Schoen FJ, Mayer JE Jr, Sacks MS. Functional collagen fiber architecture of the pulmonary heart valve cusp. Ann Thorac Surg 2009;87(4):1240–9. [PubMed: 19324159]

NIH-PA Author Manuscript

NIH-PA Author Manuscript

NIH-PA Author Manuscript

51. Kim H, Chandran KB, Sacks MS, Lu J. An experimentally derived stress resultant shell model for heart valve dynamic simulations. Ann Biomed Eng 2007;35(1):30–44. [PubMed: 17089074]
52. Kim H, Lu J, Sacks MS, Chandran KB. Dynamic Simulation of Bioprosthetic Heart Valves Using a Stress Resultant Shell Model. Ann Biomed Eng 2008;36(2):262–275. [PubMed: 18046648]
53. Kim H, Lu J, Sacks MS, Chandran KB. Dynamic simulation pericardial bioprosthetic heart valve function. J Biomech Eng 2006;128(5):717–24. [PubMed: 16995758]
54. Kirklin J, Smith D, Novick W, Naffel D, Kirklin J, Pacifico A, Nanda N, Helmcke F, Bourge R. Longterm function of cyropreserved aortic homografts: Ten year study. J Thorac Cardiovasc Surg 1993;106:154–166. [PubMed: 8320994]
55. Kunzelman KS, Cochran RP, Chuong C, Ring WS, Verrier ED, Eberhart RD. Finite element analysis of the mitral valve. J Heart Valve Dis 1993;2(3):326–40. [PubMed: 8269128]
56. Kunzelman KS, Cochran RP, Verrier ED, Eberhart RC. Anatomic basis for mitral valve modelling. J Heart Valve Dis 1994;3(5):491–6. [PubMed: 8000582]
57. Kunzelman KS, Reimink MS, Cochran RP. Flexible versus rigid ring annuloplasty for mitral valve annular dilatation: a finite element model. J Heart Valve Dis 1998;7(1):108–16. [PubMed: 9502148]
58. Lai YG, Chandran KB, Lemmon J. A numerical simulation of mechanical heart valve closure fluid dynamics. J Biomech 2002;35(7):881–92. [PubMed: 12052390]
59. Lam TV, Zubiate B, Sacks MS. Flexural properties of the aortic and pulmonary heart valve leaflets. Journal of Biomechanical Engineering. submitted
60. Lanir Y. Constitutive Equations for Fibrous Connective Tissues. Journal of Biomechanics 1983;16:1–12. [PubMed: 6833305]
61. Latif N, Sarathchandra P, Taylor PM, Antoniw J, Yacoub MH. Localization and pattern of expression of extracellular matrix components in human heart valves. J Heart Valve Dis 2005;14(2):218–27. [PubMed: 15792183]
62. Leask RL, Jain N, Butany J. Endothelium and valvular diseases of the heart. Microsc Res Tech 2003;60(2):129–37. [PubMed: 12539167]
63. Lee JM, Boughner DR, Courtman DW. The glutaraldehyde-stabilized porcine aortic valve xenograft. II. Effect of fixation with or without pressure on the tensile viscoelastic properties of the leaflet material. Journal of Biomedical Materials Research 1984;18:79–98. [PubMed: 6421823]
64. Lee JM, Courtman DW, Boughner DR. The glutaraldehyde-stablized porcine aortic valve xenograft. I. Tensile viscoelastic properties of the fresh leaflet material. Journal of Biomedical Materials Research 1984;18:61–77. [PubMed: 6699033]
65. Liao J, Vesely I. Relationship between collagen fibrils, glycosaminoglycans, and stress relaxation in mitral valve chordae tendineae. Ann Biomed Eng 2004;32(7):977–83. [PubMed: 15298435]
66. Liao J, Yang L, Grashow J, Sacks MS. The relation between collagen fibril kinematics and mechanical properties in the mitral valve anterior leaflet. J Biomech Eng 2007;129(1):78–87. [PubMed: 17227101]
67. Marella S, Krishnan S, Liu H, Udaykumar HS. Sharp interface Cartesian grid method I: An easily implemented technique for 3D moving boundary computations. Journal of Computational Physics 2005;210(1):1–31.
68. May-Newman K, Yin FC. Biaxial mechanical behavior of excised porcine mitral valve leaflets. Am J Physiol 1995;269(4 Pt 2):H1319–27. [PubMed: 7485564]
69. May-Newman K, Yin FC. A constitutive law for mitral valve tissue. J Biomech Eng 1998;120(1): 38–47. [PubMed: 9675679]
70. Mayne AS, Christie GW, Smaill BH, Hunter PJ, Barratt-Boyes BG. An assessment of the mechanical properties of leaflets from four second- generation porcine bioprostheses with biaxial testing techniques [see comments]. J Thorac Cardiovasc Surg 1989;98(2):170–80. [PubMed: 2755150]
71. Merryman WD, Bieniek PD, Guilak F, Sacks MS. Viscoelastic properties of the aortic valve interstitial cell. J Biomech Eng. in press
72. Merryman WD, Huang HY, Schoen FJ, Sacks MS. The effects of cellular contraction on aortic valve leaflet flexural stiffness. J Biomech 2006;39(1):88–96. [PubMed: 16271591]

NIH-PA Author Manuscript

NIH-PA Author Manuscript

NIH-PA Author Manuscript

73. Merryman WD, Liao J, Parekh A, Candiello JE, Lin H, Sacks MS. Differences in tissue-remodeling potential of aortic and pulmonary heart valve interstitial cells. Tissue Eng 2007;13(9):2281–9. [PubMed: 17596117]
74. Merryman WD, Youn I, Lukoff HD, Krueger PM, Guilak F, Hopkins RA, Sacks MS. Correlation between heart valve interstitial cell stiffness and transvalvular pressure: implications for collagen biosynthesis. Am J Physiol Heart Circ Physiol 2006;290(1):H224–31. [PubMed: 16126816]
75. Messier RH Jr, Bass BL, Aly HM, Jones JL, Domkowski PW, Wallace RB, Hopkins RA. Dual structural and functional phenotypes of the porcine aortic valve interstitial population: characteristics of the leaflet myofibroblast. Journal of Surgical Research 1994;57(1):1–21. [PubMed: 8041124]
76. Ming L, Zhen HK. Study of the closing mechanism of natural heart valves. Applied Mathematics and Mechanics 1986;(10):17.
77. Mirnajafi A, Raymer J, Scott MJ, Sacks MS. The effects of collagen fiber orientation on the flexural properties of pericardial heterograft biomaterials. Biomaterials 2005;26(7):795–804. [PubMed: 15350785]
78. Mirnajafi A, Raymer JM, McClure LR, Sacks MS. The flexural rigidity of the aortic valve leaflet in the commissural region. J Biomech 2006;39(16):2966–73. [PubMed: 16360160]
79. Mulholland DL, Gotlieb AI. Cell biology of valvular interstitial cells. Canadian Journal of Cardiology 1996;12(3):231–6. [PubMed: 8624972]
80. Ormiston JA, Shah PM, Tei C, Wong M. Size and motion of the mitral valve annulus in man. I. A two-dimensional echocardiographic method and findings in normal subjects. Circulation 1981;64(1): 113–20. [PubMed: 7237707]
81. Otsuji Y, Handschumacher MD, Schwammenthal E, Jiang L, Song JK, Guerrero JL, Vlahakes GJ, Levine RA. Insights from three-dimensional echocardiography into the mechanism of functional mitral regurgitation: direct in vivo demonstration of altered leaflet tethering geometry. Circulation 1997;96(6):1999–2008. [PubMed: 9323092]
82. Otto CM. Clinical practice. Evaluation and management of chronic mitral regurgitation. N Engl J Med 2001;345(10):740–6. [PubMed: 11547744]
83. Otto, CM. Valvular Heart Disease. Philadelphia: Saunders; 2004.
84. Press, WH.; Flannery, BP.; Teukolsky, SA.; Vetterling, WT. Numerical Receipes in C. Cambridge: Cambridge University Press; 1988.
85. Provenzano P, Lakes R, Keenan T, Vanderby R Jr. Nonlinear ligament viscoelasticity. Ann Biomed Eng 2001;29(10):908–14. [PubMed: 11764321]
86. Rabkin-Aikawa E, Aikawa M, Farber M, Kratz JR, Garcia-Cardena G, Kouchoukos NT, Mitchell MB, Jonas RA, Schoen FJ. Clinical pulmonary autograft valves: pathologic evidence of adaptive remodeling in the aortic site. J Thorac Cardiovasc Surg 2004;128(4):552–61. [PubMed: 15457156]
87. Rabkin-Aikawa E, Farber M, Aikawa M, Schoen FJ. Dynamic and reversible changes of interstitial cell phenotype during remodeling of cardiac valves. J Heart Valve Dis 2004;13(5):841–7. [PubMed: 15473488]
88. Rabkin E, Hoerstrup SP, Aikawa M, Mayer JE Jr, Schoen FJ. Evolution of cell phenotype and extracellular matrix in tissue-engineered heart valves during in-vitro maturation and in-vivo remodeling. Journal of Heart Valve Disease 2002;11(3):308–14. [PubMed: 12056720]discussion 314
89. Reul, H.; Talukder, N. Heart valve mechanics. The Heart; McGraw Hill: 1989.
90. Rothenburger M, Volker W, Vischer P, Glasmacher B, Scheld HH, Deiwick M. Ultrastructure of Proteoglycans in Tissue-Engineered Cardiovascular Structures. Tissue Eng 2002;8(6):1049–1056. [PubMed: 12542950]
91. Sacks MS. Biaxial mechanical evaluation of planar biological materials. Journal of Elasticity 2000;61:199–246.
92. Sacks MS. Incorporation of experimentally-derived fiber orientation into a structural constitutive model for planar collagenous tissues. J Biomech Eng 2003;125(2):280–7. [PubMed: 12751291]
93. Sacks MS, Enomoto Y, Graybill JR, Merryman WD, Zeeshan A, Yoganathan AP, Levy RJ, Gorman RC, Gorman JH 3rd. In-vivo dynamic deformation of the mitral valve anterior leaflet. Ann Thorac Surg 2006;82(4):1369–77. [PubMed: 16996935]

NIH-PA Author Manuscript

NIH-PA Author Manuscript

NIH-PA Author Manuscript

94. Sacks MS, He Z, Baijens L, Wanant S, Shah P, Sugimoto H, Yoganathan AP. Surface strains in the anterior leaflet of the functioning mitral valve. Annals of Biomedical Engineering 2002;30(10):1281–90. [PubMed: 12540204]
95. Sacks MS, Schoen FJ, Mayer JE Jr. Bioengineering Challenges for Heart Valve Tissue Engineering. Annual Review of Biomedical Engineering 2009:11.
96. Sacks MS, Smith DB, Hiester ED. The aortic valve microstructure: effects of transvalvular pressure. Journal of Biomedical Materials Research 1998;41(1):131–41. [PubMed: 9641633]
97. Sacks MS, Smith DB, Hiester ED. A small angle light scattering device for planar connective tissue microstructural analysis. Ann Biomed Eng 1997;25(4):678–89. [PubMed: 9236980]
98. Sacks MS, Yoganathan AP. Heart valve function: a biomechanical perspective. Philos Trans R Soc Lond B Biol Sci 2007;362(1484):1369–91. [PubMed: 17588873]
99. Schoen F. Aortic valve structure-function correlations: Role of elastic fibers no longer a stretch of the imagination. Journal of Heart Valve Disease 1997;6:1–6. [PubMed: 9044068]
100. Schoen F, Levy R. Tissue heart valves: Current challenges and future research perspectives. Journal of Biomedical Materials Research 1999;47:439–465. [PubMed: 10497280]
101. Schoen FJ. Cardiac valves and valvular pathology: update on function, disease, repair, and replacement. Cardiovasc Pathol 2005;14(4):189–94. [PubMed: 16009317]
102. Schwammenthal E, Chen C, Benning F, Block M, Breithardt G, Levine RA. Dynamics of mitral regurgitant flow and orifice area. Physiologic application of the proximal flow convergence method: clinical data and experimental testing. Circulation 1994;90(1):307–22. [PubMed: 8026013]
103. Simionescu DT, Lovekamp JJ, Vyavahare NR. Degeneration of bioprosthetic heart valve cusp and wall tissues is initiated during tissue preparation: an ultrastructural study. J Heart Valve Dis 2003;12(2):226–34. [PubMed: 12701796]
104. Stella JA, Liao J, Sacks MS. Time-dependent biaxial mechanical behavior of the aortic heart valve leaflet. J Biomech. 2007
105. Stella JA, Sacks MS. On the biaxial mechanical properties of the layers of the aortic valve leaflet. J Biomech Eng 2007;129(5):757. [PubMed: 17887902]
106. Sugimoto H, Sacks MS. The effects of leaflet stiffness on the dynamic geometry of the bioprosthetic aortic heart valve. Annals of Biomedical Engineering. submitted
107. Sun W, Abad A, Sacks MS. Simulated bioprosthetic heart valve deformation under quasi-static loading. Journal of Biomechanial Engineering 2005;127(6):905–914.
108. Sun W, Sacks MS. Finite element implementation of a generalized Fung-elastic constitutive model for planar soft tissues. Biomech Model Mechanobiol. 2005
109. Talman E, Boughner DR. Internal shear properties of fresh porcine aortic valve cusps: implications for normal valve function. Journal of Heart Valve Disease 1996;5(2):152–9. [PubMed: 8665007]
110. Talman EA, Boughner DR. Effect of altered hydration on the internal shear properties of porcine aortic valve cusps. Ann Thorac Surg 2001;71(5 Suppl):S375–8. [PubMed: 11388228]
111. Talman EA, Boughner DR. Glutaraldehyde fixation alters the internal shear properties of porcine aortic heart valve tissue. Annals of Thoracic Surgery 1995;60:S369–S373. [PubMed: 7646190]
112. Taylor PM, Batten P, Brand NJ, Thomas PS, Yacoub MH. The cardiac valve interstitial cell. International Journal of Biochemistry and Cell Biology 2003;35(2):113–8. [PubMed: 12479860]
113. Thom T, Haase N, Rosamond W, Howard VJ, Rumsfeld J, Manolio T, Zheng ZJ, Flegal K, O'Donnell C, Kittner S, Lloyd-Jones D, Goff DC Jr, Hong Y, Adams R, Friday G, Furie K, Gorelick P, Kissela B, Marler J, Meigs J, Roger V, Sidney S, Sorlie P, Steinberger J, Wasserthiel-Smoller S, Wilson M, Wolf P. Heart disease and stroke statistics--2006 update: a report from the American Heart Association Statistics Committee and Stroke Statistics Subcommittee. Circulation 2006;113(6):e85–151. [PubMed: 16407573]
114. Thornton GM, Frank CB, Shrive NG. Ligament creep behavior can be predicted from stress relaxation by incorporating fiber recruitment. Journal of Rheology 2001;45(2):493–507.
115. Thornton GM, Oliynyk A, Frank CB, Shrive NG. Ligament creep cannot be predicted from stress relaxation at low stress: a biomechanical study of the rabbit medial collateral ligament. J Orthop Res 1997;15(5):652–6. [PubMed: 9420592]
116. Thubrikar, M. The Aortic Valve. Boca Raton: CRC; 1990.

NIH-PA Author Manuscript

NIH-PA Author Manuscript

NIH-PA Author Manuscript

117. Thubrikar M, Bosher LP, Harry RR, Nolan SP. Mechanism of opening of the natural aortic valve in relation to the design of trileaflet prostheses. Surg Forum 1977;28:264–6. [PubMed: 617439]
118. Thubrikar M, Bosher LP, Nolan SP. The mechanism of opening of the aortic valve. J Thorac Cardiovasc Surg 1979;77(6):863–70. [PubMed: 439922]
119. Thubrikar M, Harry R, Nolan SP. Normal aortic valve function in dogs. Am J Cardiol 1977;40(4): 563–8. [PubMed: 910719]
120. Thubrikar M, Piepgrass W, Bosher L, Nolan S. The elastic modulus of canine aortic valve leaflets in vivo and in vitro. Circulation Research 1980;47:792–800. [PubMed: 7418136]
121. Thubrikar M, Piepgrass W, Deck J, Nolan S. Stresses of natural versus prosthetic aortic valve leaflets in vivo. Annals of Thoracic Surgery 1980;30:230–239. [PubMed: 7425702]
122. Thubrikar M, Piepgrass WC, Shaner TW, Nolan SP. Design and dynamic variations of aortic valve leaflets in vivo. Surg Forum 1979;30:241–3. [PubMed: 538608]
123. Thubrikar M, Piepgrass WC, Shaner TW, Nolan SP. The design of the normal aortic valve. Am J Physiol 1981;241(6):H795–801. [PubMed: 7325246]
124. Thubrikar MJ, Aouad J, Nolan SP. Patterns of calcific deposits in operatively excised stenotic or purely regurgitant aortic valves and their relation to mechanical stress. Am J Cardiol 1986;58(3): 304–8. [PubMed: 3739919]
125. Thubrikar MJ, Heckman JL, Nolan SP. High speed cine-radiographic study of aortic valve leaflet motion. J Heart Valve Dis 1993;2(6):653–61. [PubMed: 7719506]
126. Vesely I. The role of elastin in aortic valve mechanics. Journal of Biomechanics 1998;31(2):115–123. [PubMed: 9593204]
127. Vesely I, Mako WJ. Comparison of the compressive buckling of porcine aortic valve cusps and bovine pericardium. J Heart Valve Dis 1998;7(1):34–9. [PubMed: 9502137]
128. Vesely I, Noseworthy R. Micromechanics of the fibrosa and the ventricularis in aortic valve leaflets. Journal of Biomechanics 1992;25(1):101–113. [PubMed: 1733978]
129. Vigmostad S, Marella S, Lu J, Chandran K, Udaykumar HS. A Sharp Interface Technique for Fluid-Structure Interactions with Application to Tissue Heart Valves. Journal of Computational Physics. 2008Submitted
130. Vigmostad S, Udaykumar HS, Lu J, Sacks M, Chandran K. Fluid Structure Interaction Simulations of Bioprosthetic Heart Valve Dynamics Using a Sharp Interface Method. Annals of Biomedical Engineering. 2008Submitted
131. Weind KL, Ellis CG, Boughner DR. Aortic valve cusp vessel density: relationship with tissue thickness. J Thorac Cardiovasc Surg 2002;123(2):333–40. [PubMed: 11828294]
132. Wells, S.; Moeller, A. Rapid remodeling of heart valve leaflets in a bovine pregnancy model. 8th World Congress of Biomaterials; Amsterdam. 2008.
133. Weston MW, LaBorde DV, Yoganathan AP. Estimation of the shear stress on the surface of an aortic valve leaflet. Ann Biomed Eng 1999;27(4):572–9. [PubMed: 10468241]

NIH-PA Author Manuscript
NIH-PA Author Manuscript
NIH-PA Author Manuscript

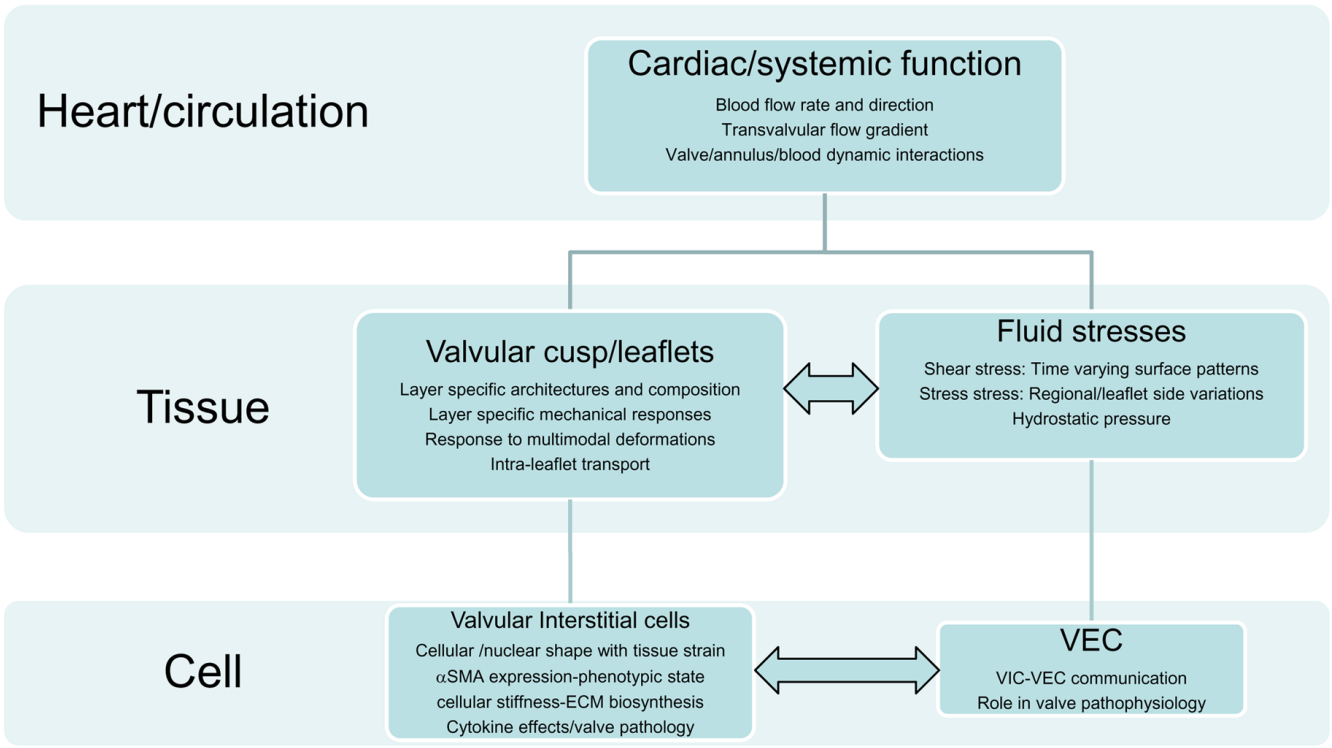

Figure 1.

A schematic approach to the biomechanics of heart valve function. As in other physiological systems, valve function can be divided into multiple length scales. While the major drivers are organ-scale hemodynamic phenomena, key to this review are underlying tissue and cellular components that facilitate and regulate these remarkable functional processes of valve function. Moreover, while this system is hierarchical, there are interactions (horizontal arrows) that have not been well described and are likely paramount in valve physiology and function.

NIH-PA Author Manuscript

NIH-PA Author Manuscript

NIH-PA Author Manuscript

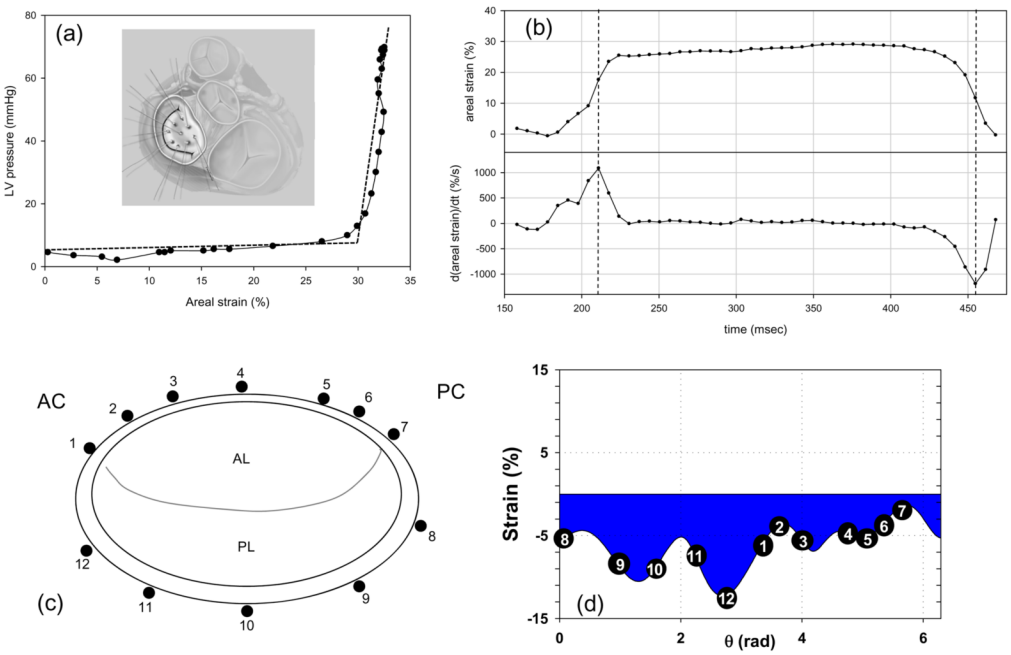

Figure 2.

(a) A representative in-vivo LV pressure-MV areal strain curve, which is analogous to a stress-strain curve for the leaflet. Here we observed a response, analogous to the classic non-linear soft tissue response, where the valve tissue undergoes large strains (up to 30% change in area) with minimal pressures, followed by a linear response highly stiff response corresponding to valve closure. Inset - A schematic of the MV anterior leaflet showing the 9 sonomicrometry transducer array. (b) Representative time-areal strain traces, along with the corresponding areal strain rate data. Strain rates were quite high, on the order of 1000%/sec. (c,d) Using similar techniques for the MV annulus, annular strains were shown to be regionally and temporally variant with stretches of −15% to 6%. This confirms the highly dynamic nature of the MV annulus and may be related to the varied fibrous-muscle structure of the annulus. Taken from (Sacks et al. 2006).

NIH-PA Author Manuscript

NIH-PA Author Manuscript

NIH-PA Author Manuscript

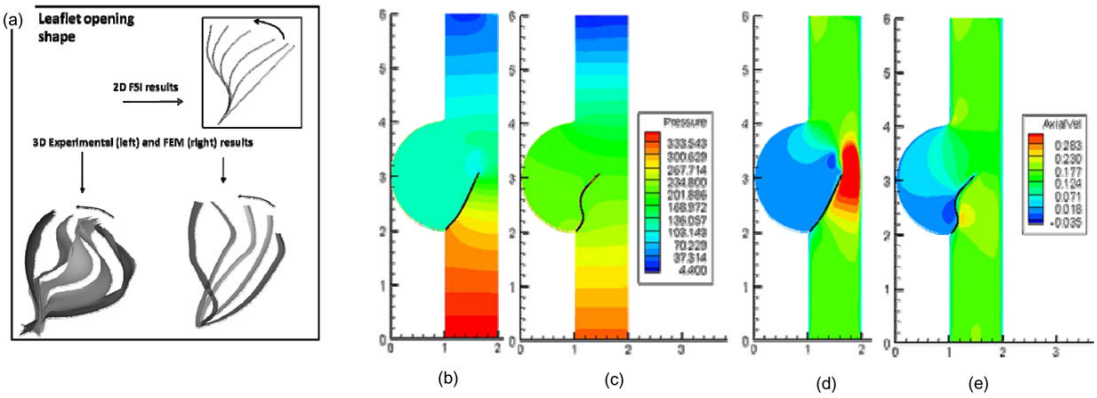

Figure 3.

(a) Stress computed during the opening phase of the cardiac cycle using experimentally determined leaflet material properties and physiologic pressure boundary conditions on the fluid. Leaflet motion computed using 2D FSI simulation (Vigmostad et al., 2008), 3D flow loop experiments (Iyengar et al., 2001), and 3D FEM computations (Kim et al., 2008). (b–e) Here, the same boundary conditions are employed for both simulations, but with different for material properties. Results showing a comparison of the pressure build-up (in Pa) with a high stiffness valve (b) and physiologic valve properties (c). In (d–e), axial velocity (in m/s) is shown for the two cases.

NIH-PA Author Manuscript
NIH-PA Author Manuscript
NIH-PA Author Manuscript

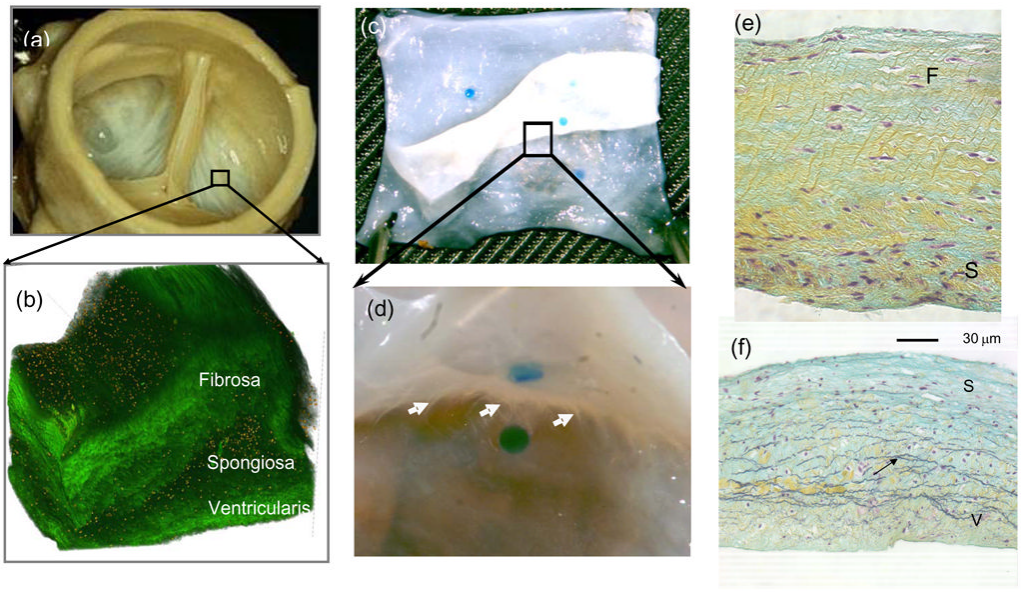

Figure 4.

(a) The AV showing, where a 1 mm × 1 mm section was removed to illustrate in (b) the 3D the tri-layered leaflet structure (Courtesy Resolution Science Corporation, CA). (c,d) A magnified view of a partially separated AV leaflet showing the numerous connections found throughout the spongiosa. (e,f) Conventional circumferential histologic cross-sections from separated AV layers, showing that the remaining spongiosa displayed no visible damage induced during separation.

NIH-PA Author Manuscript

NIH-PA Author Manuscript

NIH-PA Author Manuscript

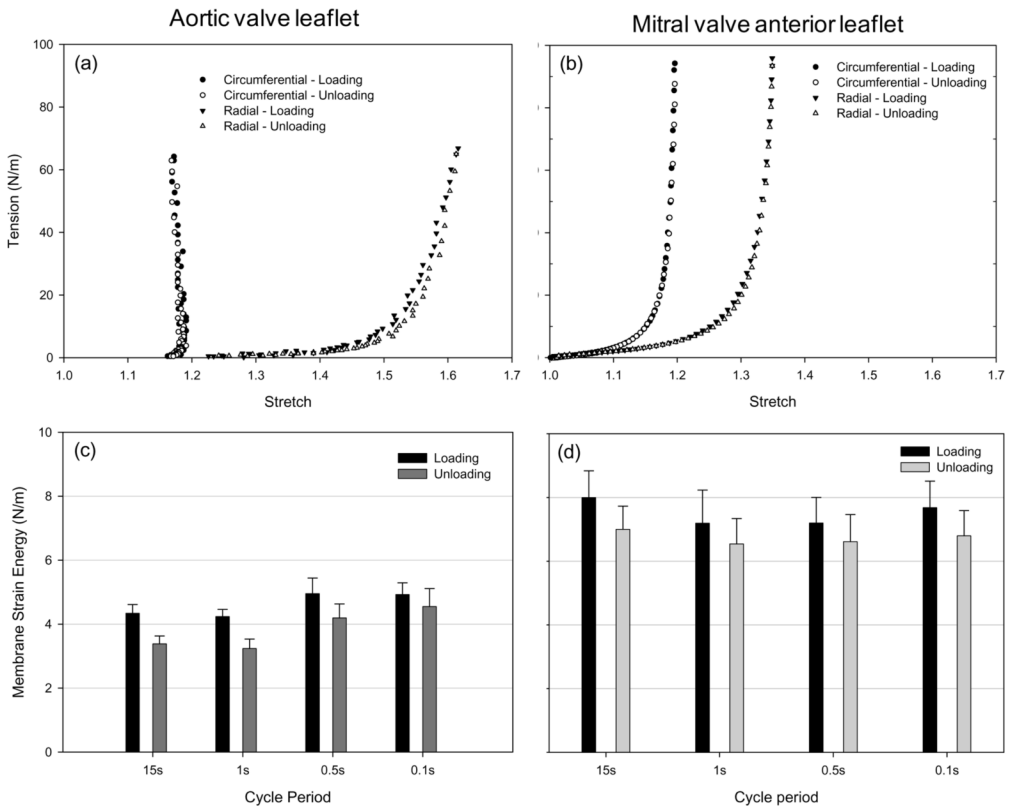

Figure 5.

Representative loading and unloading curves for the (a) AV and the (b) MVAL depicting minimal energy loss. Mean (c) AV and (d) MVAL energy storage and dissipation for all stretch rates, with hysteresis defined as the area under tension-areal stretch curve. Both leaflets demonstrated very small hysteretic losses and neither leaflet demonstrated measureable change in hysteresis with strain rate.

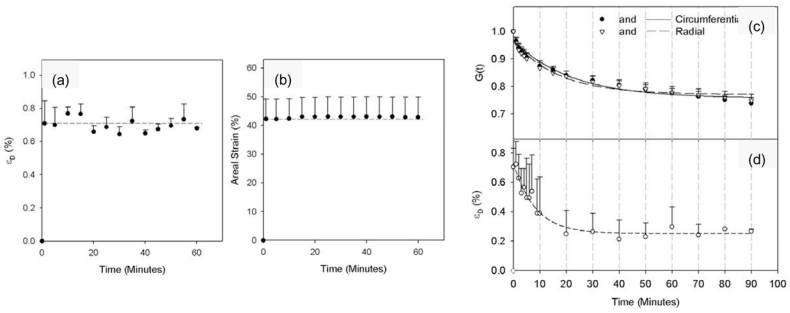

Figure 6.

Using both small angle X-ray and tissue level strain measurements of the porcine MVAL, we observed that (a) collagen fibril D-period strain (ε_D) and (b) tissue areal strain vs. time during creep tests demonstrated no detectable change with time. In contrast, biaxial stress relaxation experiments (c,d) demonstrated continued relaxation over the similar time scales. Data presented as mean±SEM

NIH-PA Author Manuscript NIH-PA Author Manuscript NIH-PA Author Manuscript

NIH-PA Author Manuscript
NIH-PA Author Manuscript
NIH-PA Author Manuscript

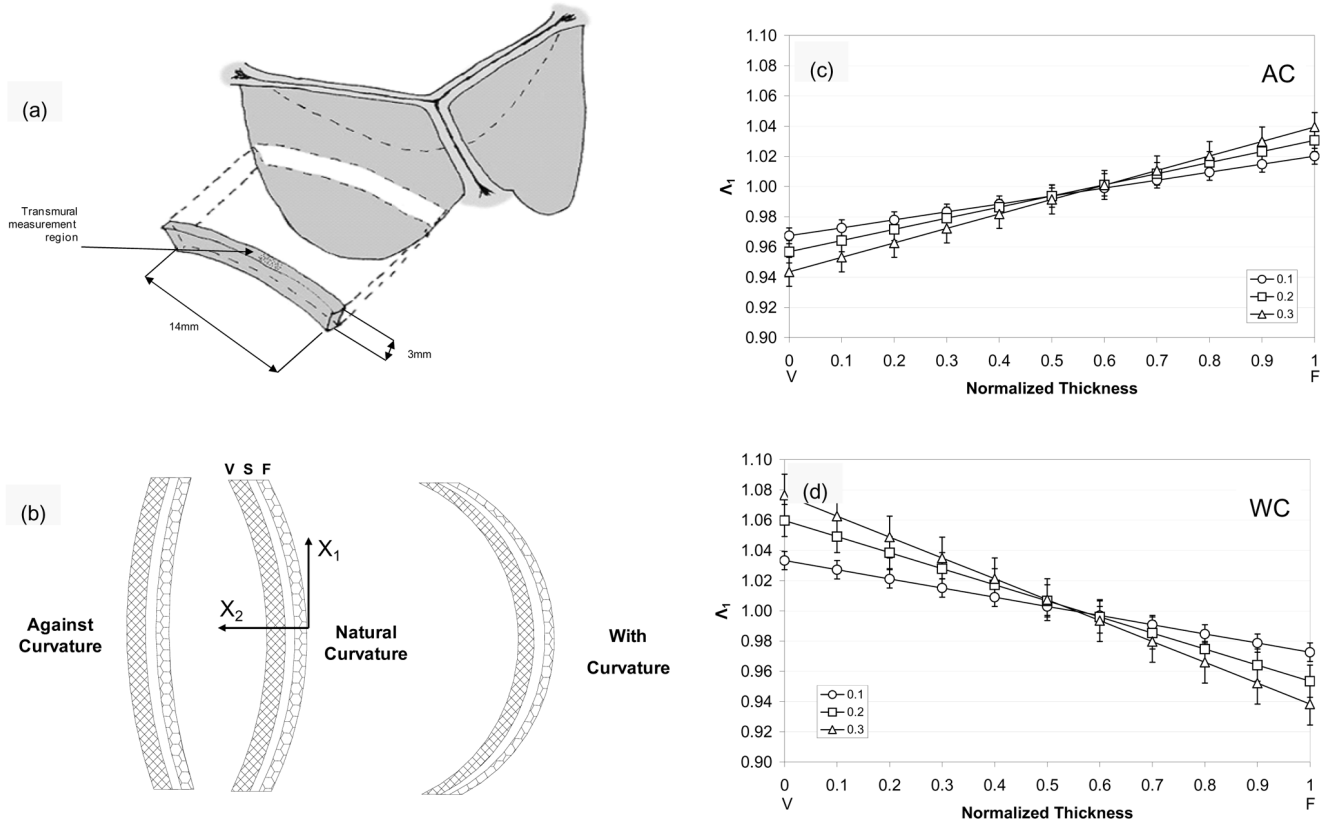

Figure 7.

Schematic showing (a) the orientation of the AV leaflet specimen used for flexural testing, including the location of the transmural measurement region, which was flexed in two directions to alternately subject the tissue layers to tension/compression (b)? The resulting transmural strain distribution of Λ_1 with increasing curvature along the normalized thickness (V=ventricularis and F=fibrosa) for the (c) AC and (b) WC directions. Here, the intersection of the composite plots with Λ_1 of 1 determined the location of the neutral axis, which was near the center and not dependent of flexural direction.

NIH-PA Author Manuscript

NIH-PA Author Manuscript

NIH-PA Author Manuscript

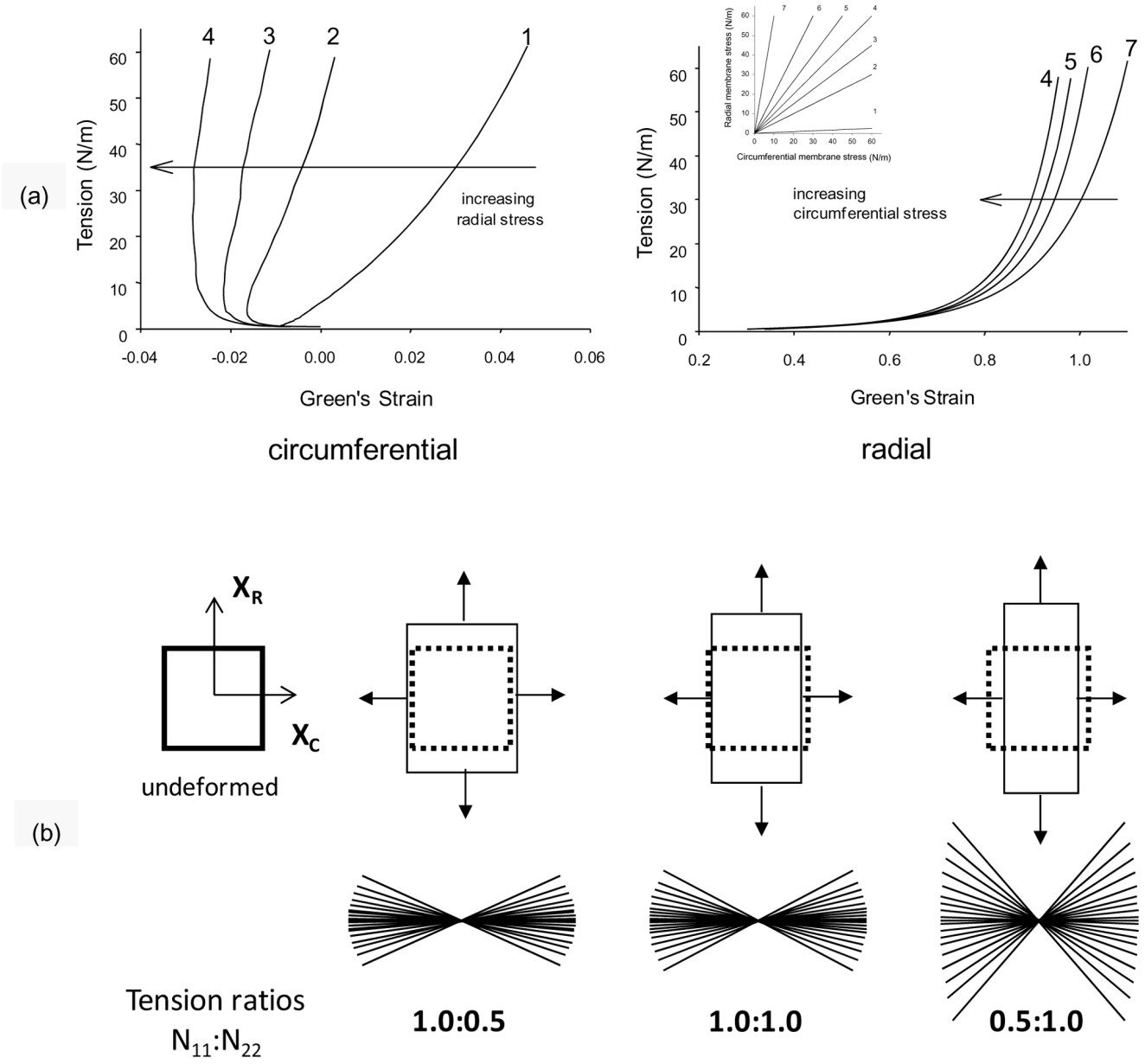

Figure 8.

(a) Representative stress-strain data in the circumferential and b) radial directions for a AV leaflet cusp demonstrating the effects of transverse loading (in-plane coupling). The underlying structural basis for this behavior is best shown by a schematic showing the fibrous structure of the cusp depicting the large collagen cords which undergo large rotations with loading (b). As the radial loads become larger with respect to the circumferential loads, the collagen fibers undergo large rotations causing contraction along the circumferential axis without buckling and allows for very large radial strains.

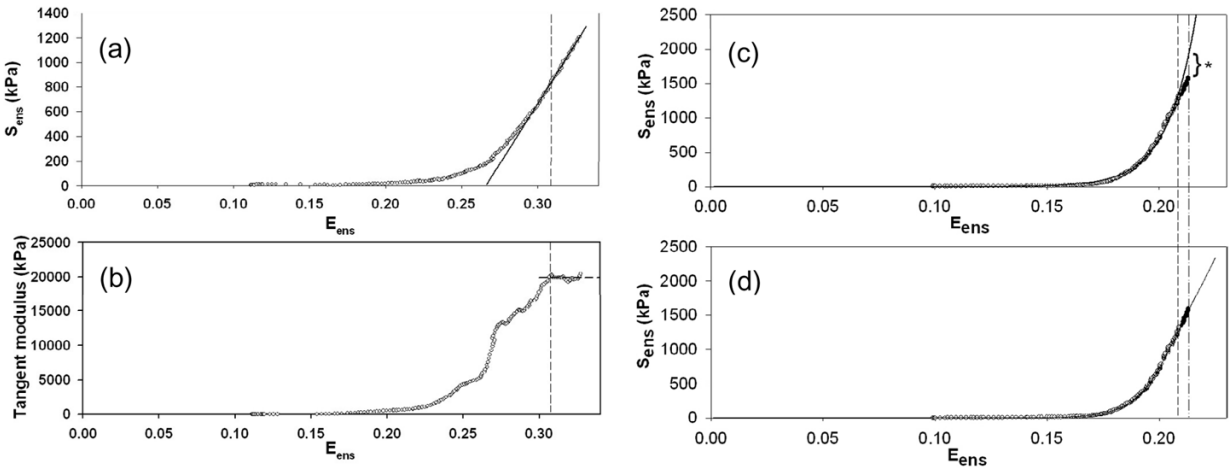

Figure 9.

(a) A representative example of the effective fiber stress-strain curve of heart valve leaflets (MVAL), showing the characteristic long toe region, transitional region, and subsequent linear region. (b) Corresponding tangent modulus of the fiber stress-strain curve. Note the sharp rise of tangent modulus in the middle of transitional region and the followed plateau that shows a constant tensile modulus in linear region. (c) The standard exponential model fitted to the data predicts a continuous increase of stiffness beyond the used data range, whereas the fiber recruitment model correctly predicates a linear stress-strain relationship beyond the used data range.

NIH-PA Author Manuscript NIH-PA Author Manuscript NIH-PA Author Manuscript

NIH-PA Author Manuscript

NIH-PA Author Manuscript

NIH-PA Author Manuscript

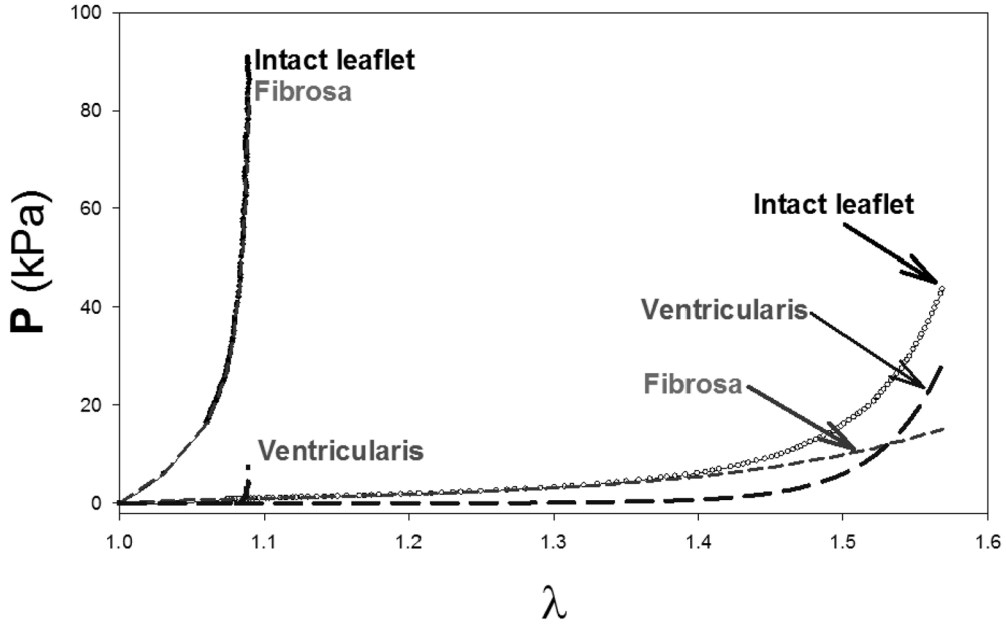

Figure 10.

Results of the 3D stress model of the AV along with the reconstructed layer stresses under physiological strains, based on biaxial experimental data taken from separated layers (Fig. 4). While the fibrosa layer clearly dominated the circumferential response, the ventricularis contributes ~2/3 of the total stress in the radial direction. Note, however, that the ventricularis only “kicks in” at radial stretches >1.4, suggesting a “over distention” protection role.

NIH-PA Author Manuscript

NIH-PA Author Manuscript

NIH-PA Author Manuscript

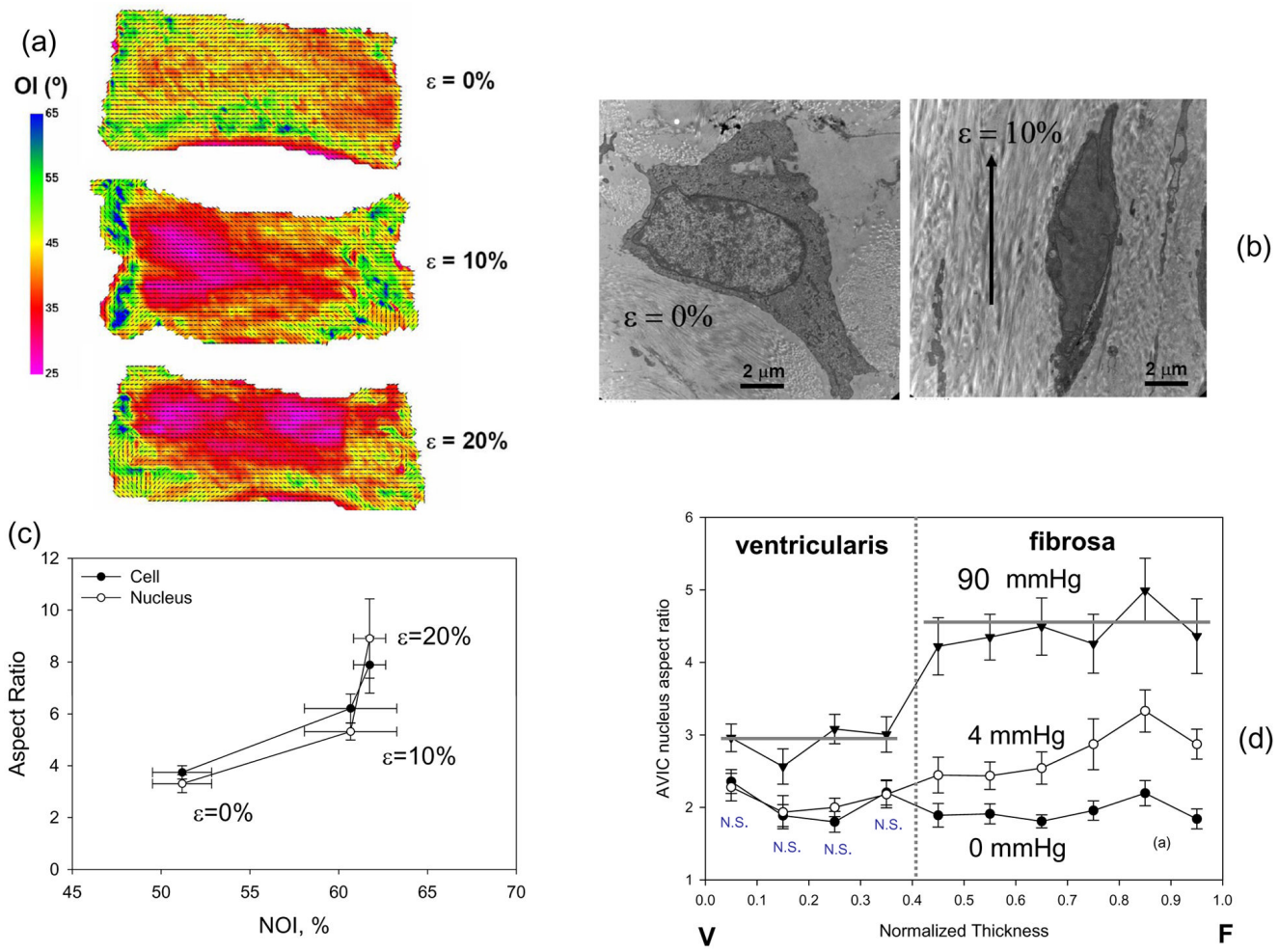

Figure 11.

(a) Collagen alignment results for circumferential strips of AV tissue subjected to 0, 10, and 20% strain. (b) Corresponding TEM images of AVICs at 0, 10, and 20% strain, with the drawn arrows show orientation of circumferential strain. (c) Both the cellular and nuclear aspect ratios changed similarly with strain and collagen alignment, supporting the use of NAR as a measure of cellular strain. In the intact valve, at 0 mmHg transvalvular pressure AVIC NAR values were uniform across the leaflet thickness In contrast, for normalized thickness positions between 0.4–1 (i.e., within the fibrosa layer) the AVIC NAR exhibited a trend of increased value with increased thickness position, approaching an average value of ~4.8 at 90 mmHg. These data indicate that AVICs in the different leaflet layers are subjected to dramatically different external stresses.

NIH-PA Author Manuscript

NIH-PA Author Manuscript

NIH-PA Author Manuscript

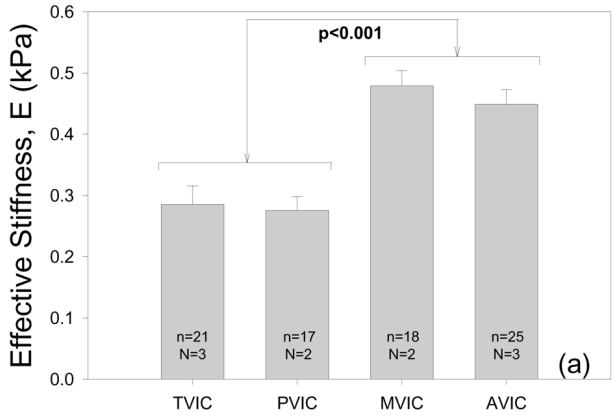

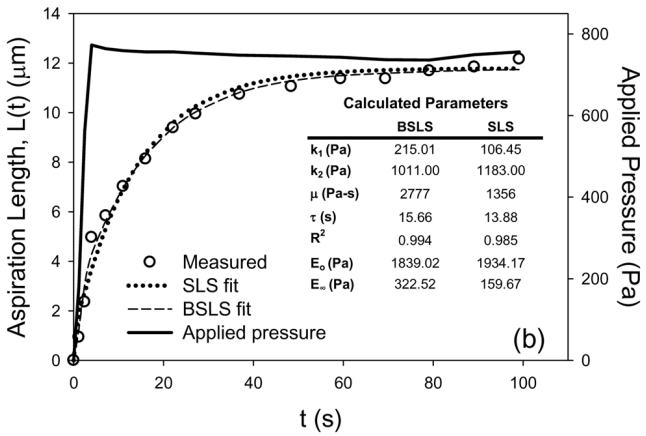

Figure 12.

(a) Using micropipette aspiration, the effective stiffness, E, of VICs from each valve demonstrated highly significant differences ($p<0.001$) in mechanical properties between the AVIC and MVIC populations and the PVIC and TVIC populations. N=hearts used and n=cells tested for each valve type. (b) Time dependent responses during the aspiration experiment for AVIC indicated that both the BSLS and SLS model fit well. Inset table shows determined parameters from both models for the representative AVIC (n=1) that was used.

NIH-PA Author Manuscript

NIH-PA Author Manuscript

NIH-PA Author Manuscript

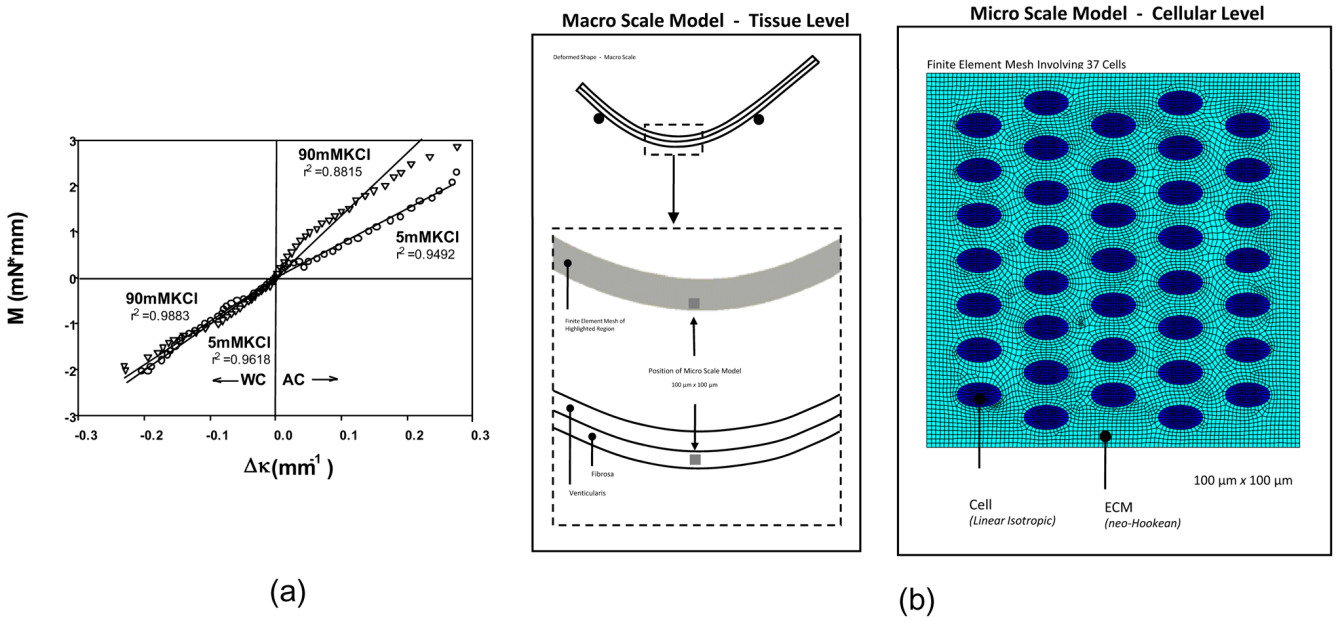

Figure 13.

(a) M vs. Δκ relations for both the AC and WC directions for specimens tested in 5 mM and 90 mM KCl, showing a highly linear response. To simulate the cellular responses in-situ a macro/micro model cellular level finite element model was developed (b). Here a bilayer model to simulate bending was utilized, the a 100 mm × 100 mm micro model utilized to estimate cellular contributions.